PURCHASE ORDER 1157300
UCX-2226
REPORT NO. HE-150-189
SERIES NO. 127-7
JUNE 5, 1961

SPONSORED BY THE
LAWRENCE RADIATION LABORATORY
UNIVERSITY OF CALIFORNIA
LIVERMORE, CALIFORNIA

TRANSIENT TEMPERATURE DISTRIBUTIONS IN A THERMALLY ORTHOTROPIC PLATE WITH NON-UNIFORM SURFACE HEATING

by

David Ross Hornbaker

A portion of a Master of Science Thesis
in Mechanical Engineering

FACULTY INVESTIGATOR:

W. H. Giedt, Professor of Aeronautical Sciences
J. Frisch, Associate Professor of Mechanical Engineering

APPROVED W. H. Giedt

DISCLAIMER

ABSTRACT

A solution is obtained for the two-dimensional transient temperature variation in a thermally orthotropic plate which is subjected to an arbitrary heating rate distribution along one face with all other surfaces being insulated. Dimensionless temperature histories and distributions determined from this solution are presented for the special, but representative, case of a linearly varying heating rate distribution on plates with varying degrees of thermal orthotropy.

These results establish quantitatively the value of a material with high planar and low normal thermal conductivities for applications where it is desired to maintain minimum temperatures on the rear or unheated surface of a heat shield when the heated surface is subjected to a very non-uniform heating rate distribution. The applicability of simplifying assumptions in analyzing such a system is discussed.

Experimental temperature measurements in a pyrolytic graphite plate heated by an oxyacetylene flame were made to verify the analytical results. Achievement of satisfactory agreement was found to be dependent upon use of thermal property values differing from those presently available for this material.* This is not unusual in that differences in production methods are known to introduce substantial property variations in anisotropic materials such as pyrolytic graphite.

*Subsequent to the completion of this study additional thermal conductivity data became available and local heat rate distributions determined more precisely. A comparison of theoretically predicted temperature distributions based on this information with experimental measurements is included in Appendix C. In view of the strong dependence of conductivity on temperature, agreement is considered satisfactory.

TABLE OF CONTENTS

NOMENCLATURE

a'	plate thickness	ft
a	transformed or real plate thickness as specified	$sec^{1/2}$ or ft resp.
C_p	specific heat	Btu/lb °F
$f(x)$	arbitrary heating distribution	Btu/ft^2 sec
F_x	Fourier number in x direction	dimensionless
F_y	Fourier number in y direction	dimensionless
$g(x)$	transformed heating distribution = $\sqrt{\alpha_{y'}}\ f\ (x\sqrt{\alpha_{x'}})/k_{y'}$	$°F/sec^{1/2}$
$H(x/\ell)$	dimensionless heating distribution (i.e., $f(x) = Q_o H(x/\ell)$)	dimensionless
k_x	thermal conductivity in x direction	Btu/ft^2 sec °F
k_y	thermal conductivity in y direction	Btu/ft^2 sec °F
K	dimensionless conductivity-geometry parameter $(k_x a^2/k_y \ell^2)$	dimensionless
ℓ'	plate length	ft
ℓ	transformed or real plate length as specified	$sec^{1/2}$ or ft resp.
$\mathcal{L}f(t)$	Laplace transform of $f(t)$	
$\mathcal{L}^{-1}f(s)$	Inverse Laplace transform of $f(s)$	
Q	heating rate	Btu/ft^2 sec
s	Laplace parameter	sec^{-1}
t	time	sec
v	temperature	°F
(x',y')	space coordinates	ft
(x,y)	transformed or real space coordinates as specified	$sec^{1/2}$ or ft resp.

α_x	thermal diffusivity $(k_x/\rho\ C_p)$	ft^2/sec
α_y	thermal diffusivity $(k_y/\rho\ C_p)$	ft^2/sec
ψ	dimensionless coordinate (x/ℓ)	dimensionless
ζ	dimensionless coordinate (y/a)	dimensionless
ρ	density	lb/ft^3

I. INTRODUCTION

Technological advance has brought about many systems which are required to operate at or are subject to high temperatures and high heat transfer rates. Aerodynamic heating of space vehicles re-entering the atmosphere and the internal heating of rocket combustion chambers and nozzles are typical examples of such systems.

Several techniques are available for protecting man and machine from these high temperatures. Basic to these are the use of heat sink materials, ablative materials, and transpiration cooling. The desire to achieve improved performance has led to the suggested development of composite materials which will permit some control of the thermal and ablative characteristics. Interest has also developed in refractory materials which have directionally oriented thermal properties in themselves. Typical of these is pyrolytic graphite. Although this material was known to Edison, specific need for its unusual properties has apparently not been sufficient to stimulate its development until now. It is thermally orthotropic in that its thermal conductivity is much greater in a plane parallel to the surface than in a plane normal to the surface.

One of the problems associated with aerodynamic heating is rapid decrease of local heat transfer with distance from a stagnation point or the point of transition to turbulent flow in the boundary layer.[8,9] This problem is alleviated by the use of an orthotropic material such as pyrolytic graphite. Consider a heat shield which has a very low thermal conductivity in the direction normal to the surface and a very high conductivity in the direction parallel to

the surface. If local hot spots occur due to stagnation conditions or transition, the heat will be conducted along the heat shield to regions of lower heat transfer rather than through the shield, which would cause local high temperatures on the inner surface.

In view of the interest in such materials the problem of predicting transient temperature distributions under the above described conditions was undertaken. In defining a system for analytical treatment the two-dimensional conduction of heat in a finite, thermally orthotropic plate was considered. To achieve similarity to conditions of practical interest, heating on one face with the other face and edges insulated were specified as boundary conditions. The heat flux was chosen as some arbitrary function of the space variable but constant with time. The solution of this problem is described in the succeeding sections and graphical presentation is made of predicted temperature histories and distributions for the case of a linearly varying heat flux and arbitrary thermal conductivities. The significance of the trends indicated is discussed.

Although the solution obtained is for a heat flux distribution which does not vary with time, it will be approximately applicable for convective heating in hypersonic flow or even low speed flow where the surface temperature is low compared with the gas temperature. This is because the flux in such cases is given by $Q = h(x)(v_{gas} - v_{surf})$, where $h(x)$ is the space dependent heat transfer coefficient, and $h(x)$ and $(v_{gas} - v_{surf})$ vary only slightly with the surface temperature, v_{surf}. The result is that Q is approximately given by $h(x)\, v_{gas}$.

To investigate the applicability of the results, experimental work was carried out using a pyrolytic graphite plate heated in an oxyacetylene flame apparatus*. This equipment provides flat plate turbulent flow convective heating for which the heat rate distribution varies essentially as the inverse 1/5 power of the distance from the leading edge. Observation of experimentally determined heating rate distributions indicated that they could be suitably approximated by a linear curve.

Temperature variations with depth, position and time were measured. The results were compared with predicted values from the above described analysis based on mean thermal properties.

*Appreciation is herewith expressed for the use of this equipment developed under University of California, Institute of Engineering Research Contract DA-04-200-ORD-776 sponsored by the U.S. Army Ballistic Missile Agency.

II. TWO DIMENSIONAL TRANSIENT CONDUCTION IN A THERMALLY ORTHOTROPIC PLATE

The two-dimensional system described in Figure 1 was considered. The plate is thermally orthotropic (i.e., in its conductivity) and oriented in such a manner that the principal conduction directions coincide with the coordinate axes (x',y'). Three surfaces are insulated, while the fourth is subjected to a non-uniform heat flux, $Q = - f(x')$, which is constant with time after the start of heating.

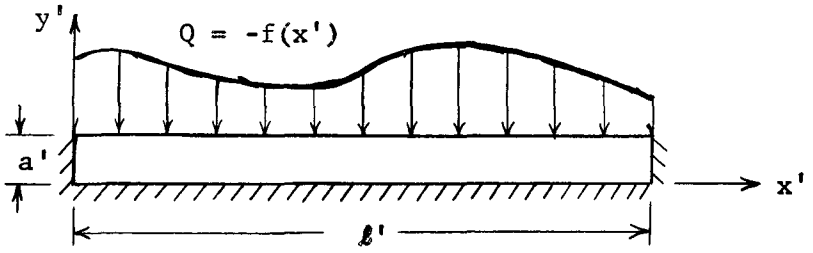

Figure 1.

The heat flux, Q, must be defined as negative, since it is assumed to flow in the negative y' direction. Primed letters are used to denote the coordinates in order to permit use of the same non-primed letters for transformed coordinates which occur much more frequently in the problem solution.

Assuming thermal properties to be constant, the two-dimensional, time dependent, heat conduction equation, with thermal diffusivities constant but having different values in the x' and y' direction, is applicable. The equation and corresponding boundary and initial conditions are then:*

$$\frac{\partial v}{\partial t} = \alpha_{x'} \frac{\partial^2 v}{\partial x'^2} + \alpha_{y'} \frac{\partial^2 v}{\partial y'^2} \qquad (1)$$

*Symbols are defined under nomenclature.

$$\frac{\partial v}{\partial x'} = 0 \qquad \text{at } x = 0,\ x = \ell' \qquad 0 \le y' \le a' \qquad (1\text{-a})$$

$$\frac{\partial v}{\partial y'} = 0 \qquad \text{at } y = 0 \qquad 0 \le x' \le \ell' \qquad (1\text{-b})$$

$$-k_{y'} \frac{\partial v}{\partial y'} = -f(x') \quad \text{at } y = a' \qquad 0 \le x' \le \ell' \qquad (1\text{-c})$$

$$v = 0 \qquad \text{at } t = 0 \qquad \begin{matrix} 0 \le y' \le a' \\ 0 \le x' \le \ell' \end{matrix} \qquad (1\text{-d})$$

In solving this system of equations, the governing partial differential equation was first simplified by introducing the following variables (x,y), which combine the space coordinates with the directional thermal properties.

$$x = \frac{x'}{\sqrt{\alpha_{x'}}} \quad , \qquad y = \frac{y'}{\sqrt{\alpha_{y'}}}$$

Equation (1) is then reduced to the transient, two-dimensional form of the conduction equation, with $\alpha = 1$.

The resulting system of equations has three independent variables x, y, and t. Application of the Laplace transformation led to

$$s\bar{v} = \frac{\partial^2 \bar{v}}{\partial x^2} + \frac{\partial^2 \bar{v}}{\partial y^2} \qquad (2)$$

$$\frac{\partial \bar{v}}{\partial x} = 0 \qquad \text{at } x = 0,\ x = \ell \qquad (2\text{-a})$$

$$\frac{\partial \bar{v}}{\partial y} = 0 \qquad \text{at } y = 0 \qquad (2\text{-b})$$

$$\frac{\partial \bar{v}}{\partial y} = \frac{g(x)}{s} \qquad \text{at } y = a \qquad (2\text{-c})$$

where g(x) denotes the heat flux distribution in the (x,y) plane and is given by $g(x) = \sqrt{\alpha_{y'}}\, f(x\sqrt{\alpha_{x'}})/k_{y'}$.

Equation (2) is now a function of only two independent variables and may be recognized as a characteristic boundary value problem. A solution may be obtained by the method of separation of variables. If it is assumed that $\bar{v} = X(x)\,Y(y)$, conventional procedures lead to the following expression, which satisfies the differential equation and boundary conditions:

$$\bar{v}(s,x,y) = \sum_{n=0}^{\infty} \frac{A_n \cos\beta x \cosh y\sqrt{\beta^2 + s}}{s\sqrt{\beta^2 + s}\,\sinh a\sqrt{\beta^2 + s}} \qquad (3)$$

$$\text{where} \quad g(x) = \sum_{n=0}^{\infty} A_n \cos\frac{n\pi x}{\ell}$$

$$\beta = \frac{n\pi}{\ell} \qquad n = 0,\ 1,\ 2,\ \ldots$$

Inversion of equation (3) must now be performed. The reader is referred to Appendix A for details of the procedure followed. The resulting equation is,

$$v(t,x,y) = \sum_{n=0}^{\infty}\sum_{i=0}^{\infty} A_n \cos\beta x \int_0^t \frac{\exp(-\beta^2 t)}{\sqrt{\pi\, t}} \left[\exp\left(-\frac{b_1^2}{4t}\right) + \exp\left(-\frac{b_2^2}{4t}\right)\right] dt \qquad (4)$$

where: $b_1 = [(2i + 1)a - y]$

$b_2 = [(2i + 1)a + y]$

$i = 0,\ 1,\ 2,\ \ldots$ (a summation index)

Equation (4) was integrated termwise. When the resulting expression is transformed back to the original variables x' and y' and the primes dropped for convenience, the final and complete solution is:

$$v(t,x,y) = \sum_{i=0}^{\infty} \frac{\sqrt{\alpha_y}}{k_y} B_o \left\{ \frac{2\sqrt{t}}{\sqrt{\pi}} \left[\exp\left(- \frac{[(2i+1)a-y]^2}{4\,\alpha_y\, t} \right) + \exp\left(- \frac{[(2i+1)a+y]^2}{4\,\alpha_y\, t} \right) \right] \right.$$

$$\left. - \frac{(2i+1)a-y}{\sqrt{\alpha_y}} \operatorname{erfc}\left(\frac{(2i+1)a-y}{2\sqrt{\alpha_y\, t}} \right) - \frac{(2i+1)a+y}{\sqrt{\alpha_y}} \operatorname{erfc}\left(\frac{(2i+1)a+y}{2\sqrt{\alpha_y\, t}} \right) \right\}$$

$$+ \sum_{n=1}^{\infty} \sum_{i=0}^{\infty} \frac{\sqrt{\alpha_y}\, B_n\, \ell \cos \frac{n\pi x}{\ell}}{k_y\, 2n\pi \sqrt{\alpha_x}} \left\{ \exp\left(- \frac{[(2i+1)a-y]n\pi \sqrt{\alpha_x}}{\ell \sqrt{\alpha_y}} \right) \left[1 + \operatorname{erf}\left(\frac{n\pi \sqrt{\alpha_x\, t}}{\ell} - \frac{(2i+1)a-y}{2\sqrt{\alpha_y\, t}} \right) \right] \right.$$

$$- \exp\left(+ \frac{[(2i+1)a-y]n\pi \sqrt{\alpha_x}}{\ell \sqrt{\alpha_y}} \right) \operatorname{erfc}\left(\frac{n\pi \sqrt{\alpha_x\, t}}{\ell} + \frac{(2i+1)a-y}{2\sqrt{\alpha_y\, t}} \right) + \exp\left(- \frac{[(2i+1)a+y]n\pi \sqrt{\alpha_x}}{\ell \sqrt{\alpha_y}} \right) \cdot$$

$$\left. \left[1 + \operatorname{erf}\left(\frac{n\pi \sqrt{\alpha_x\, t}}{\ell} - \frac{(2i+1)a+y}{2\sqrt{\alpha_y\, t}} \right) \right] - \exp\left(\frac{[(2i+1)a+y]n\pi \sqrt{\alpha_x}}{\ell \sqrt{\alpha_y}} \right) \operatorname{erfc}\left(\frac{n\pi \sqrt{\alpha_x\, t}}{\ell} + \frac{(2i+1)a+y}{2\sqrt{\alpha_y\, t}} \right) \right\} \tag{5}$$

where $f(x) = \sum_{n=0}^{\infty} B_n \cos \frac{n\pi x}{\ell}$

This expression has been shown to satisfy the differential equation and its boundary and initial conditions by substitution. The convergence of the series involved has not been rigorously established. Numerical calculations, however, indicate that if they do converge, they converge rapidly.

It is of interest to note in the inversion to the real time domain (see Appendix A) that a restriction was put on the range of variation of the Laplace parameter, s. It might be expected that this would limit the range of time over which the solution is valid, since s and t are related. This must not be the case, however, since the solution has been shown to satisfy all of the required conditions.

Noteworthy also is the fact that no restrictions have been put on $f(x)$, the heat rate distribution. For example, it may take on values such that there is heat lost in some areas of the plate and heat gained in other areas. Although this is not of importance under the circumstances for which this solution was desired, it may be useful in other applications. The solution is also valid for the case of a finite width line source normal to the (x,y) plane, such that $f(x)$ describes the width of the line source and the remaining portion of the surface is considered insulated.

III. EXPRESSION OF SOLUTION IN TERMS OF DIMENSIONLESS PARAMETERS

As given by equation (5), the solution involves four significant variables, x, y, t, and the ratio of the conductivities in the x and y directions. If this ratio is chosen as $\alpha_x a^2/\alpha_y \ell^2$, it relates the thermal properties and body dimensions and is at the same time dimensionless. The remaining variables can be non-dimensionalized in the usual fashion.

Letting $\psi = \frac{x}{\ell}$, $\zeta = \frac{y}{a}$ (dimensionless coordinates)

and $F_x = \frac{\alpha_x t}{\ell^2}$, $F_y = \frac{\alpha_y t}{a^2}$ (dimensionless times or Fourier numbers),

it can be seen that the parameter relating thermal properties and body dimensions is simply the ratio of the Fourier numbers. It will be denoted by

$$K = \frac{F_x}{F_y} = \frac{k_x a^2}{k_y \ell^2}$$

It will also be desirable to non-dimensionalize the heat flux distribution $f(x)$ by putting it in the form $f(x) = Q_o H(x/\ell)$. Q_o will then represent the magnitude of the flux, while $H(x/\ell)$ represents the shape of the distribution such as $\sin \frac{\pi x}{\ell}$ or $(1 - x/\ell)$ for a linear variation. This introduces a term $Q_o \left(\frac{t}{\rho C_p k_y}\right)^{1/2}$ which is common to all terms on the right hand side of equation 5). It is therefore convenient to divide both sides by this quantity, therefy defining a dimensionless temperature, $v/Q_o \left(\frac{t}{\rho C_p k_y}\right)^{1/2}$.

Using these non-dimensional parameters, equation (5) becomes:

$$\frac{v}{Q_o\left(\frac{t}{\rho\, c_p k_y}\right)^{1/2}} = 2C_o \sum_{i=0}^{\infty} \left\{ \frac{1}{\sqrt{\pi}} \left[\exp\left(-\frac{(2i+1-\zeta)^2}{4F_y}\right) + \exp\left(-\frac{(2i+1+\zeta)^2}{4F_y}\right)\right] \right.$$

$$\left. - \left[\frac{2i+1-\zeta}{2\sqrt{F_y}} \operatorname{erfc}\left(\frac{2i+1-\zeta}{2\sqrt{F_y}}\right) + \frac{2i+1+\zeta}{2\sqrt{F_y}} \operatorname{erfc}\left(\frac{2i+1+\zeta}{2\sqrt{F_y}}\right)\right]\right\}$$

$$+ \sum_{n=1}^{\infty}\sum_{i=0}^{\infty} \frac{C_n \cos n\pi\psi}{2n\pi\sqrt{F_x}} \left\{ \exp\left[-\sqrt{K}n\pi(2i+1-\zeta)\right] \left[1 + \operatorname{erf}\left(n\pi\sqrt{F_x} - \frac{2i+1-\zeta}{2\sqrt{F_y}}\right)\right]\right.$$

$$- \exp\left[\sqrt{K}n\pi(2i+1-\zeta)\right] \operatorname{erfc}\left(n\pi\sqrt{F_x} + \frac{2i+1-\zeta}{2\sqrt{F_y}}\right) + \exp\left[-\sqrt{K}n\pi(2i+1+\zeta)\right] \cdot$$

$$\left.\left[1 + \operatorname{erf}\left(n\pi\sqrt{F_x} - \frac{2i+1+\zeta}{2\sqrt{F_y}}\right)\right] - \exp\left[\sqrt{K}n\pi(2i+1+\zeta)\right] \operatorname{erfc}\left(n\pi\sqrt{F_x} + \frac{2i+1+\zeta}{2\sqrt{F_y}}\right)\right\} \tag{6}$$

where $H\left(\frac{x}{\ell}\right) = \sum_{n=0}^{\infty} C_n \cos\frac{n\pi x}{\ell} = \frac{f(x)}{Q_o}$

IV. CHARACTERISTICS OF THE SOLUTION

The solution as presented in equations (5) and (6), although apparently complex, is composed of logical elements. The first and most obvious of these is the single series first term. This term is independent of x and contains only the zeroth term of the Fourier expansion for $f(x)$. This term must then account for a constant heat flux over all x. The solution for the constant flux case is well known. Reference 1, page 112, gives two possible solutions for this case, one of which is

$$v(t,y) = \frac{2Q(\alpha t)^{1/2}}{k} \sum_{n=0}^{\infty} \left[\text{ierfc} \left(\frac{(2n+1)a-y}{2\sqrt{\alpha t}} \right) + \text{ierfc} \left(\frac{(2n+1)a+y}{2\sqrt{\alpha t}} \right) \right] \quad (7)$$

where Q is the constant heat rate. The only properties of concern in this case will of course be those in the y direction since a constant heat rate eliminates any effect of the x directional properties.

It may be shown, performing the indicated integrations in equation (7) by parts, that the single series first term is identically equal to equation (7) when Q equals B_o in equation (5) or $Q_o C_o$ in equation (6). This single series term will henceforth be referred to as the constant flux term.

The physical significance of the constant flux term can be seen if the meaning of the zeroth Fourier expansion coefficient of any arbitrary function is considered. This coefficient is the mean ordinate of the function such that the integral of the function over the interval of interest is equal to the coefficient times the interval length. The constant flux term therefore represents the temperature distribution due to the total net heat rate evenly distributed over the plate.

Consider now the case where k_x is infinite. The double series can be shown to go to zero such that the constant flux term is again the solution. This is to be expected since no gradient in the x direction could be supported and the heat input would be evenly distributed in an infinitesimal thickness at the surface. This infinite conductivity condition is the ideal one for dissipation of hot spots. How closely a material approaches this condition is a measure of its usefulness in such a proposed application. The magnitude of the constant flux term compared with the remainder of the solution is therefore of interest.

Another limiting case of interest is that of k_x being zero. With this restriction, the local temperature would be independent of the heat rate at any other point and the value of the temperature would therefore be directly proportional to the local heat rate. Although this is concluded from physical reasoning, it can also be shown from the analytical expression. Substitution of $k_x = 0$ into the expression causes the double series term to be indeterminate. It can be shown that the indeterminate form reduces to the expected result by the use of L'Hospital's rule.

It is somewhat surprising that, regardless of the form of $f(x)$, the x dependence of the solution appears only in the terms $\cos n\pi x/\ell$. This fact simplifies numerical calculations considerably in that the temperature may be computed for any point (x_1,y_1) and the value of the temperature at any x along y_1 may then be obtained by a simple cosine modification of the double series term.

This characteristic is of particular significance when the flux varies linearly along the plate. The Fourier expansion of such a function

has only the zero and odd coefficients. This means that at the point $x/\ell = 1/2$, $\cos n\pi x/\ell$ is always zero. The temperature for any value of y at this x/ℓ is then independent of the degree of orthotropy and is given by the constant flux term.

As is often the case in conduction solutions of this type the temperature tends to be proportional to $\sqrt{t}$ as t becomes large. It may also be noted that the temperature is directly proportional to the flux magnitude such that superposition may be utilized.

V. THE EFFECT OF ORTHOTROPY ON TEMPERATURE DISTRIBUTION

The importance of the degree of orthotropy exhibited by a material in a specific application will, in general, depend on the imposed heating rate distribution and the plate dimensions. Since the number of possible heating distributions is infinite it was necessary to select a significant and representative case for further investigation. Various degrees of orthotropy and a range of plate dimensions could then be compared for this particular case.

It was desirable to choose a distribution for the heat flux which could be used to approximate as many practical cases as possible and at the same time one which lent itself to visualization of the controlling mechanisms. A simple linear variation of the form $Q_o(1 - x/\ell)$ appeared to satisfy these requirements and was therefore chosen. Due to the direct dependence of temperature on heat rate, dimensionless similarity exists and Q_o serves only to fix the magnitude of the temperature but not the distribution. Consequently, moderate to extreme heat rate variations will be essentially included in the results when Q_o is used as a multiplying factor.

A. Temperature Distributions

The dimensionless form of the temperature expression, equation (6), was used. The Fourier coefficients were obtained for the term $H(x/\ell) = (1 - x/\ell)$ by standard methods[3]. Temperature history at various points (ψ, ζ) was then evaluated and plotted in the form shown in Figures 2, 3, and 4 with the property-geometry term, K, as a parameter. Cross plots were prepared of temperature variations with position as shown in Figures 5, 6, 7, and 8. Discussion of these presentations follows.

Values of K were chosen on the basis of experimental specimens which were 6" x 1/4" in size. For this geometry K values of 1.6×10^{-3}, 0.1, and 0.4 correspond to conductivity ratios of approximately 1, 60, and 225, respectively.

Although equation (6) appears quite formidable to evaluate numerically, the properties of the error function and the values of the coefficients C_n reduce the task to a reasonable magnitude. The value of the error function is effectively 1 for all arguments greater than 2.5. It can be seen that as n and i take on values greater than 2 the error function terms are constant for reasonable values of F_y and these terms tend to cancel each other, thereby making the effect of higher order terms extremely small. The coefficients C_n at the same time become small, even further reducing higher terms. These results also strongly suggest the convergence of the series involved.

As was previously pointed out, the linear flux distribution leads to temperatures at $\psi = 1/2$ which are independent of K. This property will give a common point to all distributions which may be plotted for various values of K in the ψ direction at a given ζ. Ease in evaluation of the effect of K results. The curves in Figures 5, 6, and 7 showing the temperature distributions at the unheated surface, the mid-plane, and the heated surface for values of time corresponding to $F_y = 0.5$ and 1.0 illustrate this point.

It may be noted that limiting values of zero and infinity were not placed on K but rather on k_x. Limiting values of K do not tell whether k_x or k_y is the controlling term and the solution is highly dependent on which case is being considered. For example, $K = \infty$ can

represent either $k_x = \infty$ or $k_y = 0$. The case of $k_y = 0$ is the adiabatic wall problem which does not fit the conditions for which the solution was obtained, while $k_x = \infty$ is a valid consideration. Similarly, $k_y = \infty$ leads to a fin problem which should be solved with a source term in the differential equation. The boundary conditions used here do not encompass this case but do include the possibility of k_x being zero.

Values of time corresponding to $F_y = 1.0$ were chosen for Figures 2 through 8 in order to graphically expand the initial period during which the temperatures change more rapidly. Curves for several locations (ψ, ζ) have also been plotted for values of time up to $F_y = 4.0$ and are presented in Appendix B, Figures A-1 to A-9. The curves shown there for $\psi = 1/2$ and $\zeta = 0, 1/2$ and 1, and for $\psi = 1$ and $\zeta = 0, 1/2$ and 1, were obtained from the corresponding curves at $\psi = 0$. The double series part of the solution contains ψ only in the $\cos n\pi\psi$ terms, the remainder being independent of ψ. Once this series is evaluated at a given value of ζ, only the change in $\cos n\pi\psi$ is required to determine the variation of temperature at that value of ζ. Calculation of the variation of temperature at any value of ψ is therefore comparatively straightforward.

Figures 5, 6, and 7, showing temperature distributions along ψ, were prepared using this simple cosine modification. The resulting temperature distributions consequently have a cosine form. Figure 8 showing temperature distributions through the thickness of the plate (i.e., along ζ), was prepared by cross plotting from Figures 5, 6, and 7.

B. Discussion of Calculated Temperature Distributions

In comparing orthotropic materials one extreme would be a material with an infinite thermal conductivity in the direction parallel to the heated plane (i.e., k_x), the other extreme would be zero conductivity along this plane. The conductivity normal to this plane would be held constant for comparison. It might be expected that an isotropic material would be a compromise between these limiting cases. If relatively thin plates with length to thickness ratios of the order twenty five are involved,* however, it can be seen that this is far from true. Instead, Figures 2, 3, and 4 show that the temperature histories in an isotropic plate ($K = 1.6 \times 10^{-3}$) follow very closely those of a material for which $k_x = 0$. Geometry is thus seen to be an important parameter. In order therefore to see the effects of thermal property variation only the above mentioned geometry will be considered in this discussion.

At the unheated surface (Figure 2) the temperature history for $K = 0.4$ (conductivity ratio of 225) is not unlike that for a material with $k_x = \infty$ except for extremely early values of time. This means that for the assumed geometry a material with these properties will be effective in distributing the uneven heating while materials with conductivity ratios of less than 60 ($K = 0.1$) will be relatively poor.

The effect of K on the temperature at the heated surface (Figure 4) is strongly dependent on time. At the instant heating is initiated the temperature is independent of K because there is a time lag before local heating effects can be transmitted into and along the plate (this is a minor effect at the unheated surface). Consequently,

*This is the approximate geometry on which the values of K were selected.

the temperature initially depends only on the local heat rate. As time increases the dependence on K increases and the trends become the same as those on the unheated surface.

The temperature variations along the unheated surface shown in Figure 5 may be of special interest. This figure demonstrates the effectiveness of high planar conductivity. At $F_y = 1.0$ the temperature distribution for $K = 0.4$ varies a maximum of only 13 per cent from that for a material with $k_x = \infty$, whereas for an isotropic material the maximum temperature is approximately 100 per cent higher. In applications where high temperatures are undesirable the advantage of using orthotropic materials becomes obvious. Figures 6, 7, and 8 further illustrate the above points as the heated surface is approached. They indicate, however, that the degree of orthotropy is less effective in alleviating the heating near the heated surface.

The question of what approximations may be made in the analysis of the behavior of highly orthotropic materials without serious errors may occur in practical studies. Based on the results of this study a reasonable answer would have been obtained for $K = 0.4$ if the flux distribution had been assumed uniform and equal to the average value. As was pointed out above, the error would have been a maximum of 13 per cent at $F_y = 1.0$ on the unheated surface. The error would have been larger nearer the heated surface but this is not important if the objective is to reduce the rear temperatures.

Two possible approximations appear to have merit when treating other than linear heating variations. The first is simply to assume a constant average flux as was just described. This is limited to highly

orthotropic materials and to heating variations of order one. The second and more exact is to approximate the distribution by a constant plus a superimposed linear variation. The properties described previously for highly orthotropic materials indicate that this procedure would yield satisfactory accuracy. If this method is chosen, the solution is readily available in the curves presented here. Most heating distributions of engineering importance will lend themselves to this approach. If suitably precise property values are available, results to the desired degree of accuracy for any complex problem could of course be determined with the aid of an electronic computer.

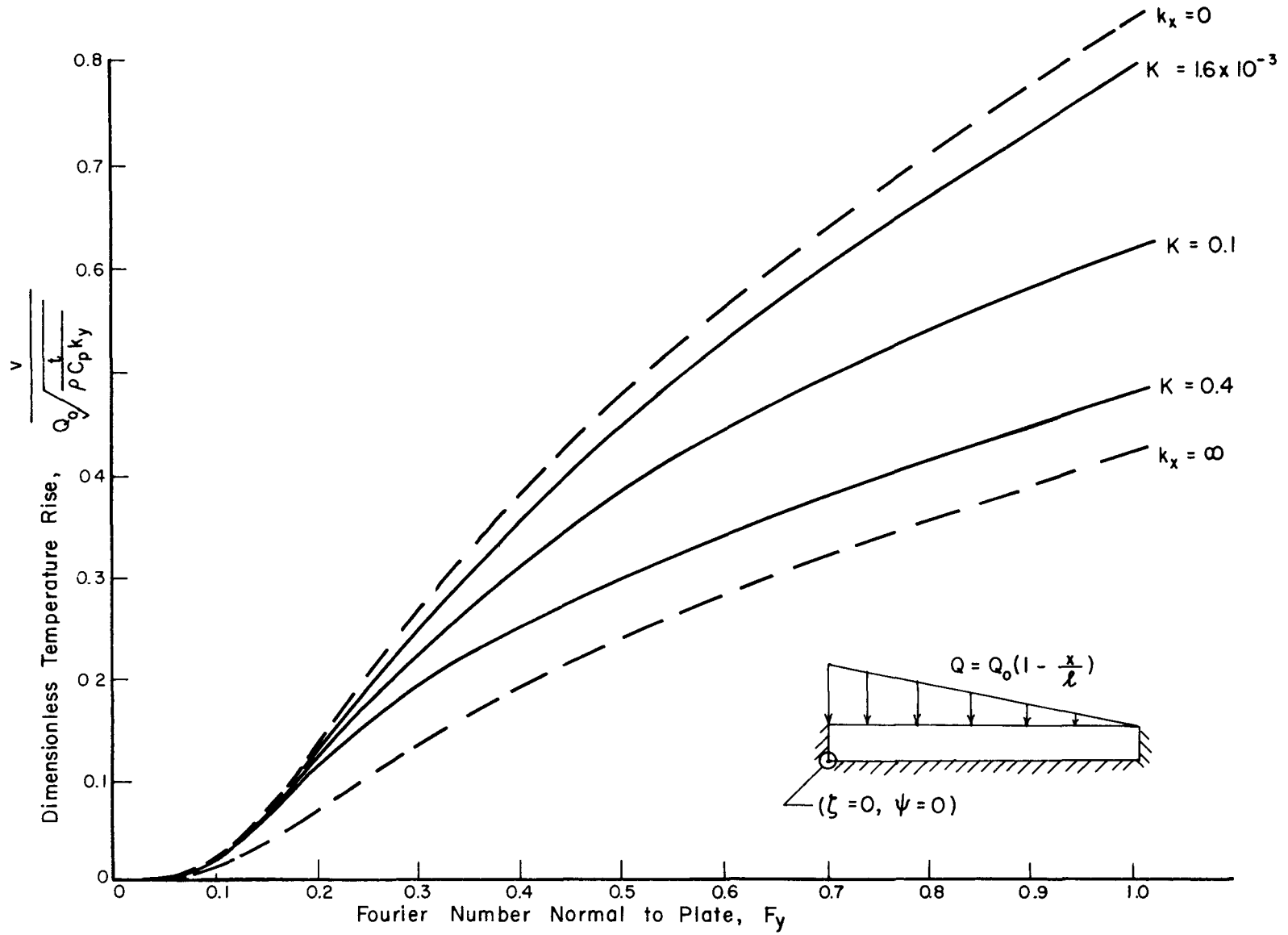

FIGURE 2 - PREDICTED TEMPERATURE VARIATION AT LEADING EDGE OF UNHEATED SURFACE

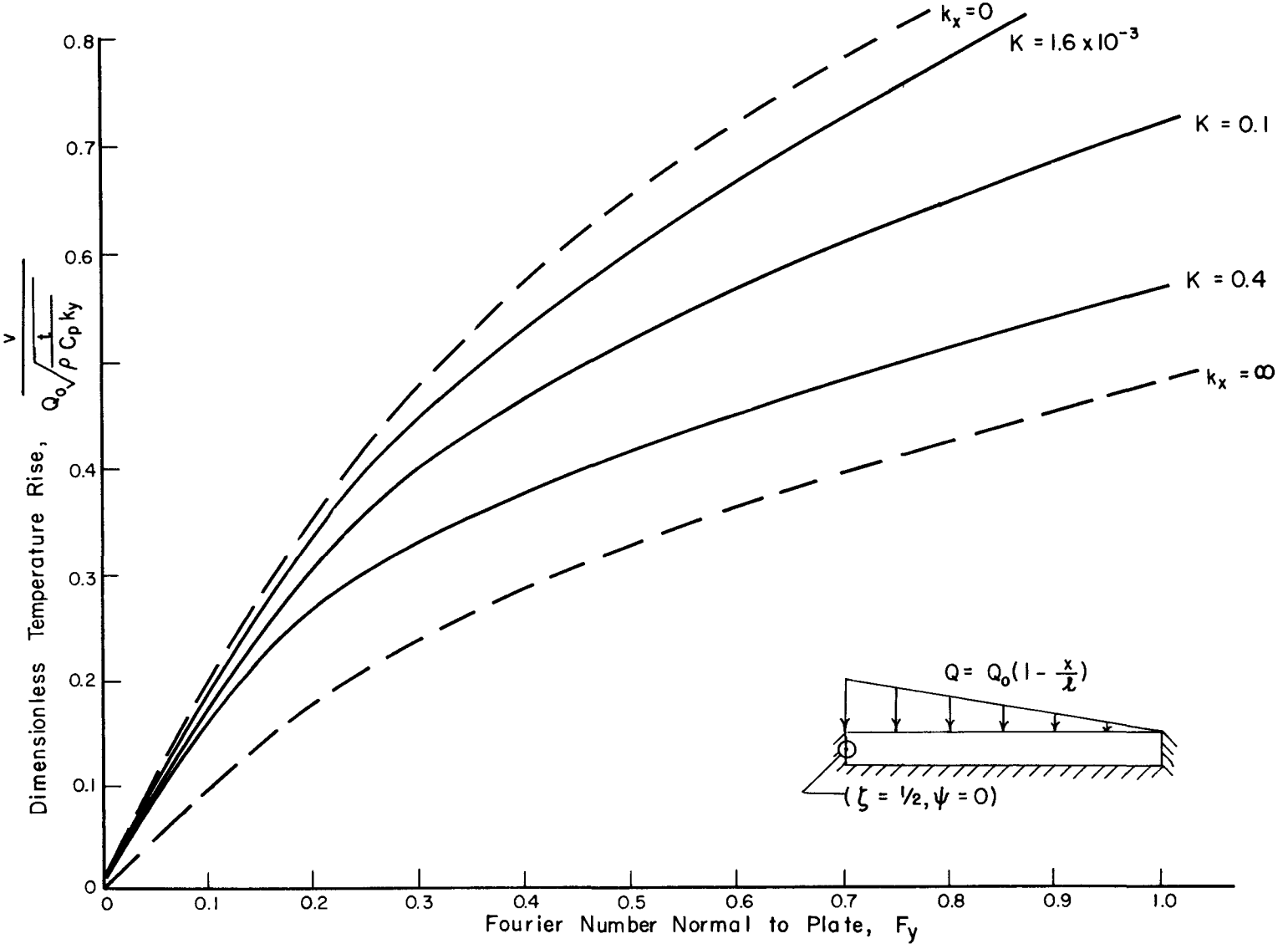

FIGURE 3 - PREDICTED TEMPERATURE VARIATION AT LEADING EDGE OF MIDPLANE

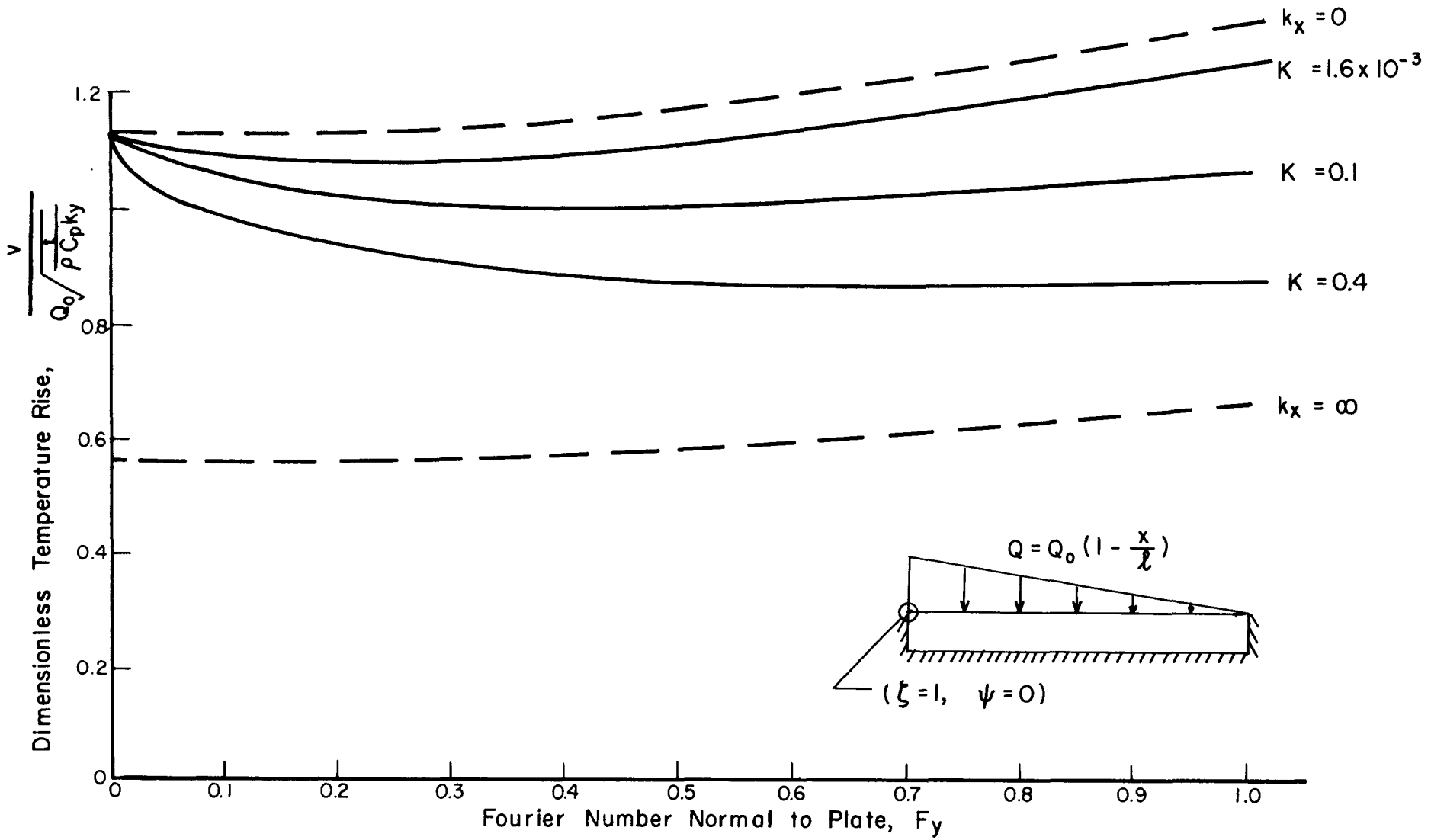

FIGURE 4 - PREDICTED TEMPERATURE VARIATION AT LEADING EDGE OF HEATED SURFACE

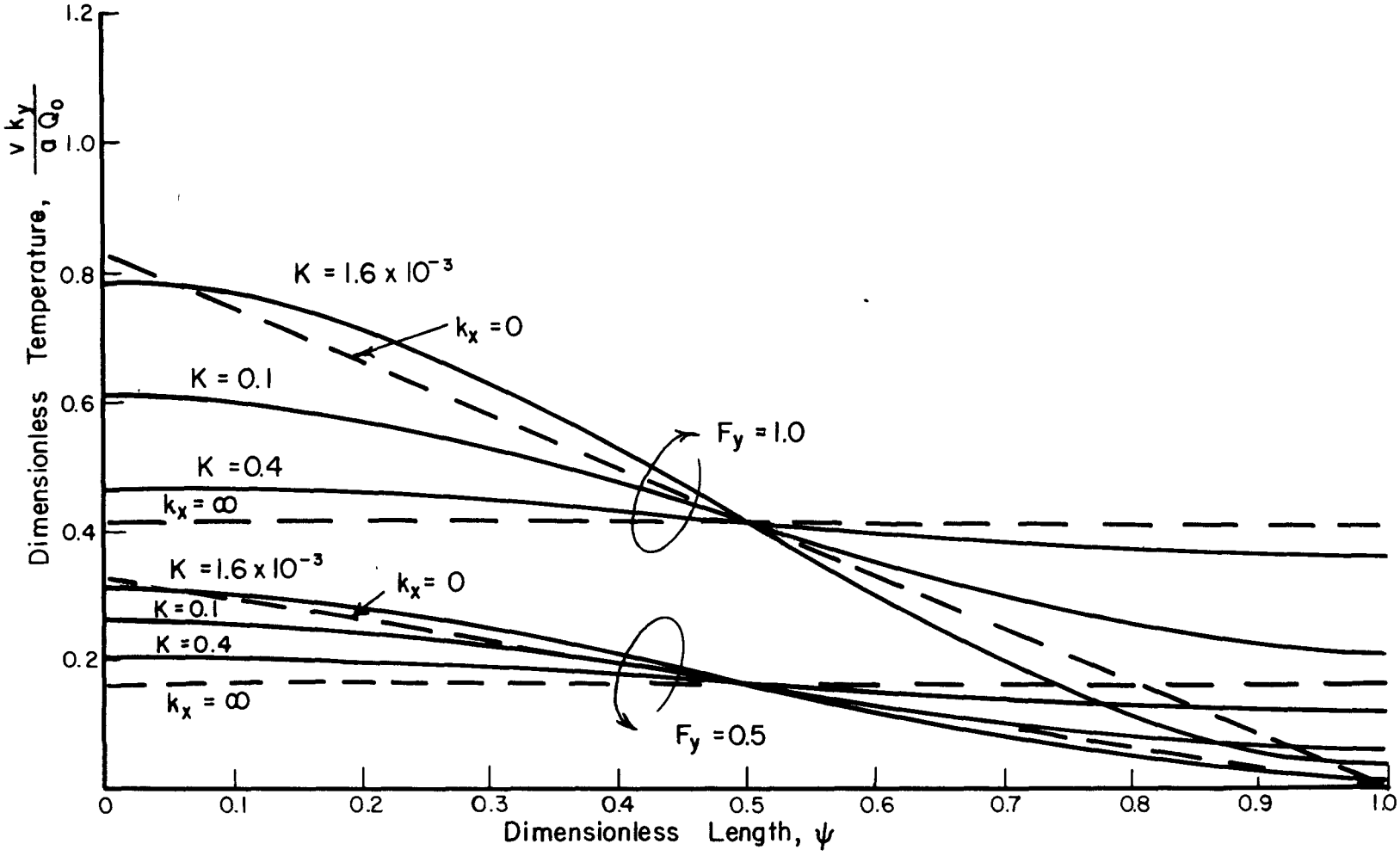

FIGURE 5 - PREDICTED TEMPERATURE DISTRIBUTION ALONG UNHEATED SURFACE

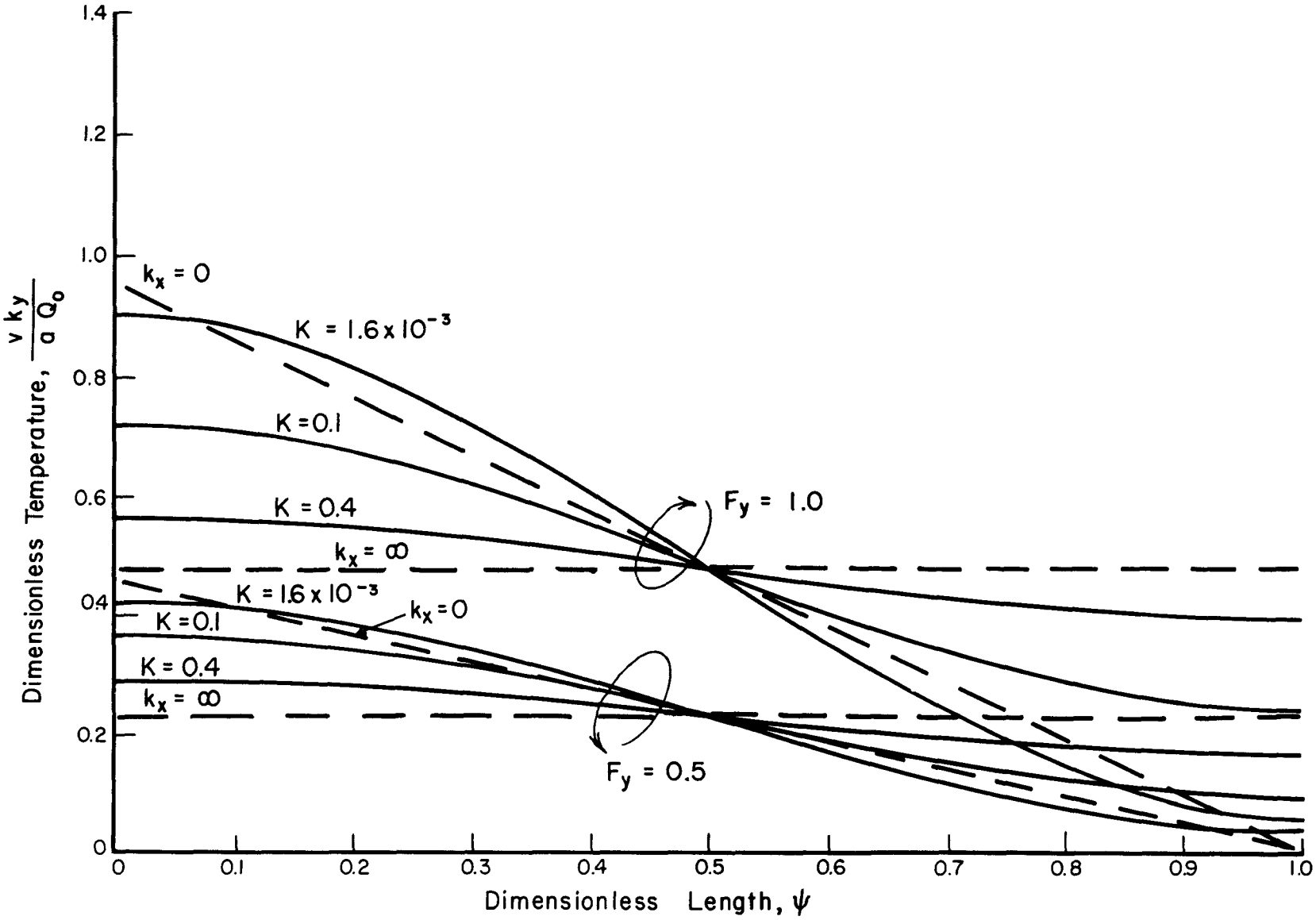

FIGURE 6 - PREDICTED TEMPERATURE DISTRIBUTION ALONG MIDPLANE

HXD 7549

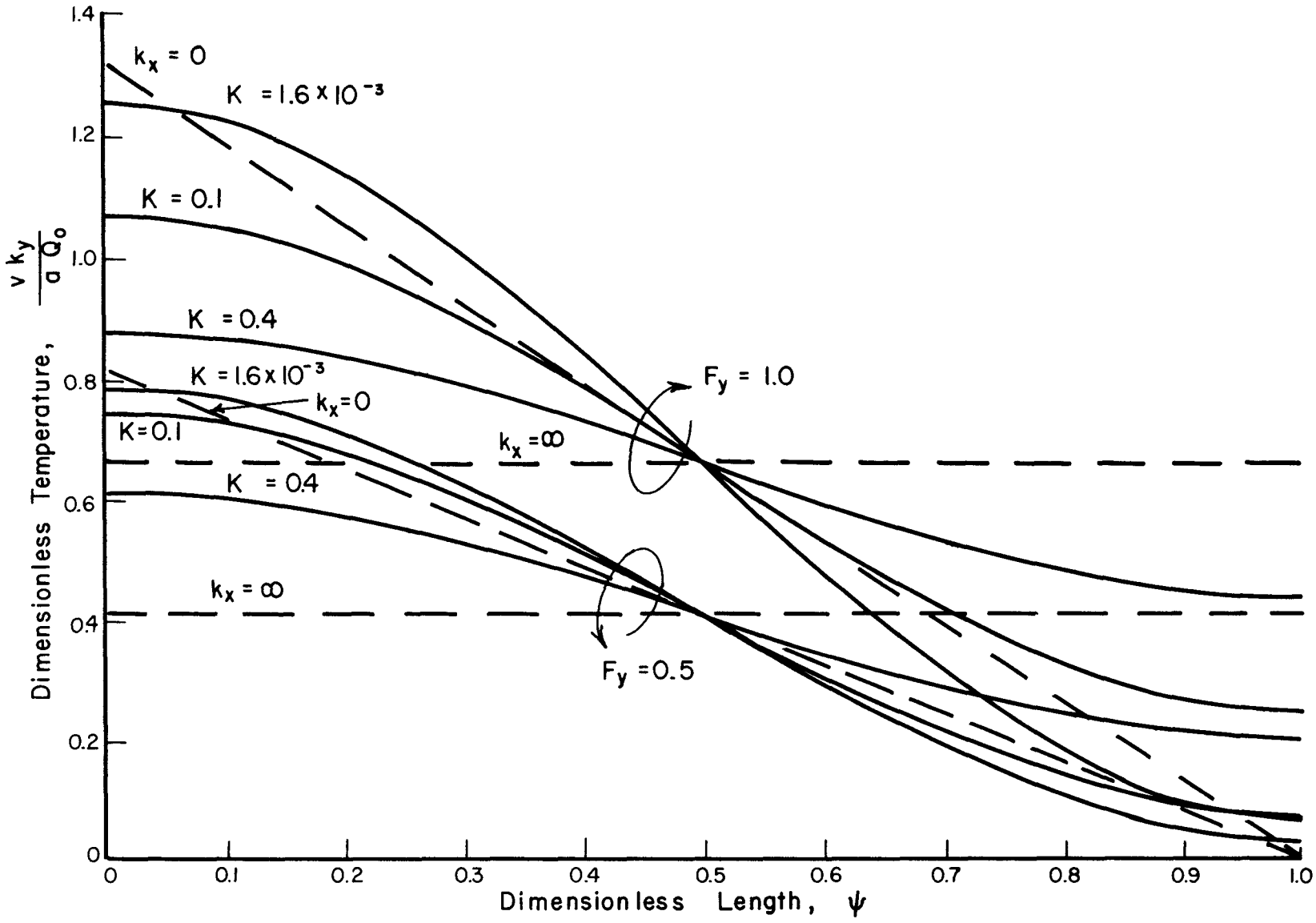

FIGURE 7 - PREDICTED TEMPERATURE DISTRIBUTION ALONG HEATED SURFACE

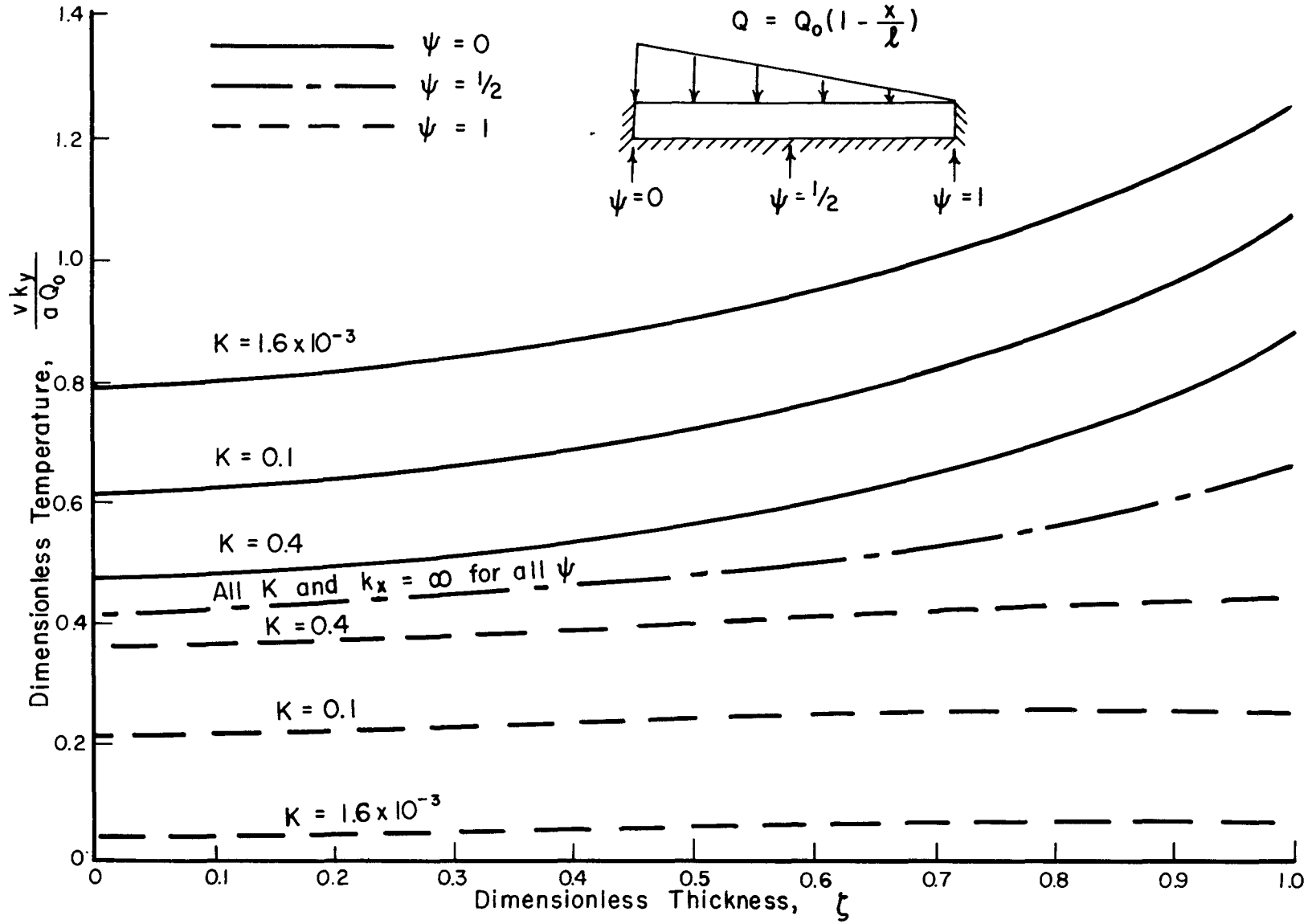

FIGURE 8 - PREDICTED TEMPERATURE DISTRIBUTION THROUGH PLATE AT $F_y = 1.0$

VI. EXPERIMENTAL INVESTIGATION

For experimental verification of the theoretical results obtained temperature variations were measured in a 6" x 4" x 1/4" pyrolytic graphite plate subjected to convective heating from an oxyacetylene flame. The characteristics of the heating apparatus, details of the test plate instrumentation and test procedure are described in the following sections.

A. Heating Apparatus

The heating of one surface of the pyrolytic graphite plate was accomplished by mounting it on the top of the open section of the oxyacetylene flame apparatus shown in Figure 9.[4] This equipment consists of an oxyacetylene torch with associated fuel sources and water cooled exhaust system. The torch contains thirty separate nozzles arranged in a rectangle approximately 1-1/2" x 3". The sides and bottom of the test section were made of refractory brick lined with ordinary commercial graphite.

The heating characteristics of the flame flowing though the test section have been investigated previously.[5,6] Results (see Figures 11 and 12) show that the heating rate distribution is similar to that along a flat plate parallel to a hot gas stream. The presence of atomic hydrogen in the flame, however, substantially influences the local heat transfer, particularly near the leading edge. This causes more variation along the plate, which was advantageous for the present study.

B. Test Plate Instrumentation

The test specimens used were 6" x 4" x 1/4" plates of pyrolytic graphite. This material is highly orthotropic with a thermal conductivity ratio of approximately 250. The properties are strongly dependent on temperature and a mean must be chosen for comparison to the analytical.

Due to the physical characteristics of pyrolytic graphite, instrumentation for temperature measurement is difficult. Thermocouples cannot be spot welded to the surface, nor can they be peened into slots or holes as in a metallic surface. The technique used was that of spring loading a thermocouple directly onto the surface. A thermocouple was placed in a 1/8" diameter, two hole, ceramic tube. The junction was adjusted such that it lay across the end of the tube between the holes and was effectively the only part of the thermocouple protruding. The ceramic tube was then placed in a steel sleeve which in turn fitted into a second sleeve which contained a compression spring. A series of these devices was attached to a plate which could be raised and lowered to compress the springs. A load of up to eight pounds could be applied. The assembled configuration is shown in Figure 10.

In order to measure temperatures through the thickness of the plate small flat bottomed holes were milled in the plate to the desired depth to accept the ceramic thermocouple tube. It was felt that due to the extremely high conductivity in the plane of the plate the effect of the hole on the surrounding temperature distribution would be small.

The thermocouples used were 32 gauge chromel-alumel. Their outputs were recorded on a twelve channel Minneapolis-Honeywell recording oscillograph.

C. Test Procedure

The plate was placed in the test section with the leading edge about 1/8" above and 1/4" downstream of the top row of nozzles. A series of eight thermocouples was arranged along the centerline of the plate parallel to the flow to measure the temperature distribution on the unheated surface. The flame was turned on and the plate heated for a period of approximately 90 seconds. The test was then repeated measuring temperatures along a line normal to the centerline two inches from the leading edge while holding two thermocouples in their original position. These two thermocouples were then checked against the first test to assure reproducibility.

Four holes were then milled at distances of 7/8, 1-1/2, 3, and 5-3/4 inches from the leading edge along the centerline of the plate to a depth of 0.050". With thermocouples now against the bottoms of these holes the test was repeated with the same two thermocouples in their fixed positions on the unheated surface. The holes were made progressively deeper until a depth of 0.220" was reached. Further depths were not possible without breaking through the plate. In each case the two surface thermocouples were checked against the original surface temperatures and the test rerun if sufficiently accurate reproduction was not attained.

VII. EXPERIMENTAL RESULTS

It was determined that in the course of the thirteen tests run the unheated surface reference temperatures were reproduced to ±6%. This deviation was attributed to slight uncontrollable changes in fuel flow rate and to changes in the flow configuration as the graphite lining eroded away.

Temperature distributions measured normal to the direction of flow, across the unheated surface, indicated that the heat flow in the plate was very nearly two-dimensional. The maximum temperature drop measured was 25° F one inch from the centerline. Since the system is symmetrical about the centerline the gradients across the plate at this line should be extremely small. The effect of any deviation from two-dimensional conduction would be to lower the temperatures.

Although the local heat transfer coefficient distribution along the test plate does not vary significantly with time, the temperature difference between the hot gas and the heated surface decreases with time and as a result the heat rate decreases. The heating rate distributions for average surface temperatures of 1200 and 1600 °F are shown in Figures 11 and 12. As can be noted the change in heating rate distribution for these two conditions is small. During the course of the tests the surface temperature fell within the range for which these curves apply from an elapsed time of 5 to 40 seconds. It was therefore concluded that the heating could be considered constant during most of the test.

Experimental measurements of temperature distributions through the plate and along the length of the plate are shown in Figures 13, 14, 15, and 16 at an elapsed time of 20 seconds. This time was chosen as

representative since the constant heating is well established and radiation from the unheated surface is still negligible.

The temperatures measured 1/4" from the trailing edge were found to be consistently higher than those just upstream. This was attributed to either unusual turbulence near this point or conduction through a small piece of graphite which was in contact with the trailing edge.

VIII. COMPARISON OF THEORETICAL AND EXPERIMENTAL RESULTS

In order that the curves presented in Section V-B could be used to predict the temperatures it was necessary to approximate the experimental heating by a linear curve. The chosen distribution has been included in Figures 11 and 12. It is of the form $Q_1 + Q_2(1 - x/\ell)$ where $Q_1 = 15$ Btu/ft^2 sec and $Q_2 = 30$ Btu/ft^2 sec.

Temperatures were taken from the dimensionless theoretical curves by first letting $Q_1 = Q_0$ in Figures 2, 3, and 4, and taking the appropriate value from the curve for $k_x = 0$. Q_2 was then set equal to Q_0 and temperatures chosen from the curve for $K = 0.4$. The two values were then summed to give the predicted temperature.

The thermal conductivities of pyrolytic graphite are stongly dependent upon density and temperature. Curves taken from reference 7 are shown in Figure 17. The specific gravity of the test specimen was measured to be 2.25 so a mean conductivity, k_y, was chosen as 1.61×10^{-4} Btu/ft sec °F. The specific heat was taken to be 0.45 Btu/lb °F. The value of $K = 0.4$ was considered to represent a reasonable average.

Due to the temperature being independent of K at $x/\ell = 1/2$ it was decided to first make a comparison at this point. Figure 13 shows a plot of the temperature distribution through the plate at an elapsed time of 20 seconds with the corresponding analytical values using the above properties.

As can be seen the agreement is not very good. Several reasons for this were considered: a) incorrect values for the heat flux, b) errors in experimental temperature measurement, c) non two-dimensional conduction,

and d) incorrect property values. Since the temperatures are directly proportional to heat flux the analytical curve would be everywhere either high or low if the error is in the heat flux. This is clearly not the case. Although some errors are inherent in the method of temperature measurement, these would lead to values which are lower than the actual but not low in some areas and high in others. The same reasoning holds for the possibility of three-dimensional conduction. These conclusions lead to the assumption that the mean conductivity chosen was in error or that a mean will not produce a valid prediction due to the extreme dependence on temperature.

To further substantiate the accuracy of the value used for the heat flux it was noted that, for constant specific heat, the integral of the experimental and analytical curves should be the same if the proper heating rate had been chosen. The integrals were found to agree within 4%.

A higher value of thermal conductivity is required to cause the analytical curve to approach the experimental. Trial and error methods were therefore used to determine an effective conductivity which would cause the two curves to fall close together. It was found that a value k_y of 4.56×10^{-4} Btu/ft sec °F gave a reasonable correlation. In order to determine the time range over which this new value of conductivity is good it was used to predict the distributions at 10 and 40 seconds. These comparisons also appear in Figure 13. It appears that the new value is valid over most of the test period, although it begins to deviate by t = 40 seconds. Figures 14 and 15 show similar correlations near the leading and trailing edge.

In all cases, the analytical curves are low at the surface. This is to be expected, since the conductivity is low at higher temperatures and steeper gradients are required to maintain the heat flux at the heated surface.

Cross plotting the above described curves produces distributions along the length of the plate as shown in Figure 16. These curves further show the effect of low conductivity in the high temperature zone near the heated surface. As was previously noted, the temperatures measured near the trailing edge were consistently high. For this reason the curves in Figure 16 are not well established near the trailing edge.

The above comparisons indicate that the thermal conductivity of the test specimen was higher than expected although a similar variation with temperature probably existed. The higher conductivity may be attributed to differences in manufacturing process. Since the conductivities shown are so highly dependent upon density and temperature it does not seem unreasonable that different manufacturers will produce material with different conductivities under similar conditions.

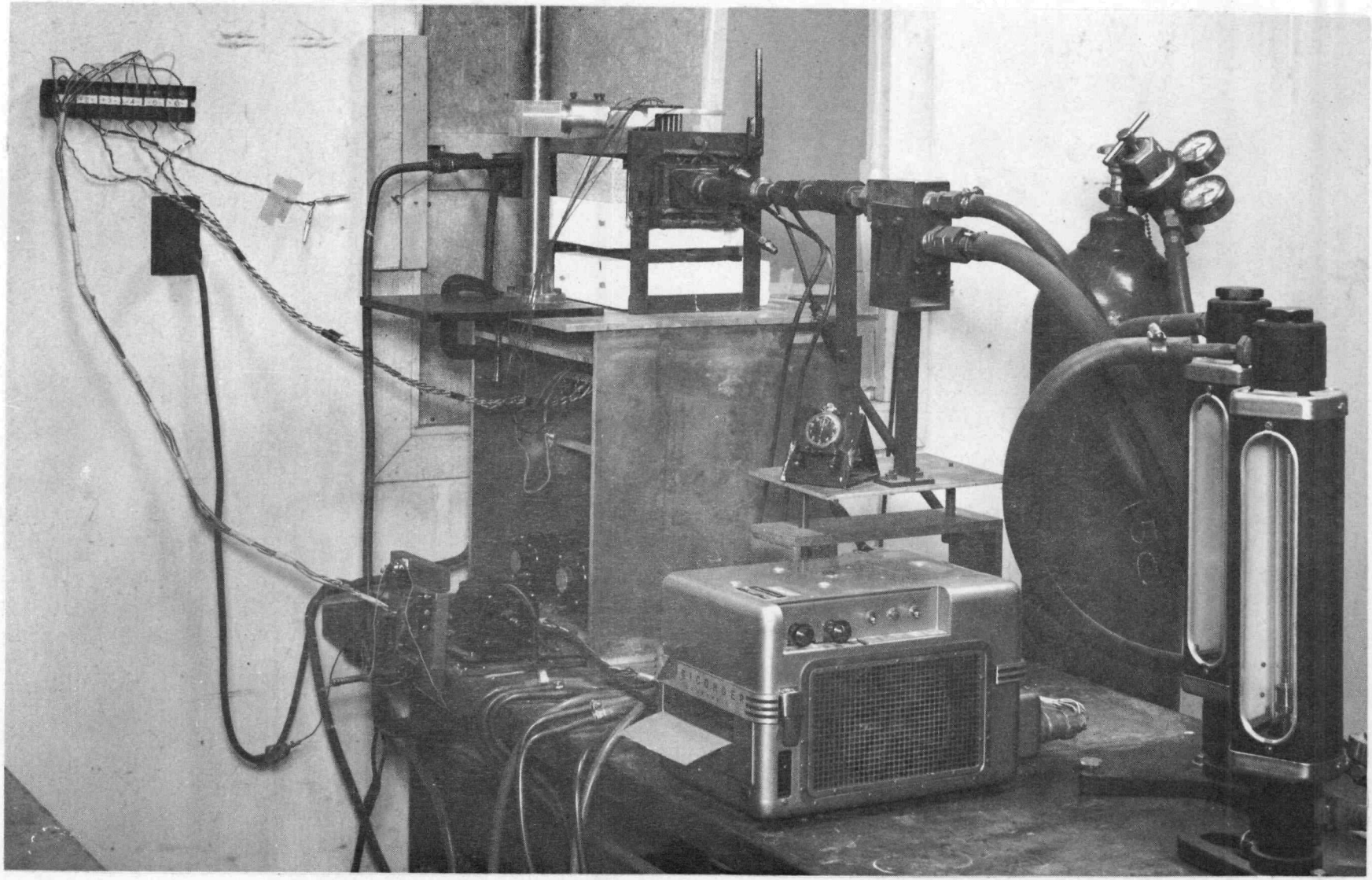

FIGURE 9 - SURFACE HEATING APPARATUS

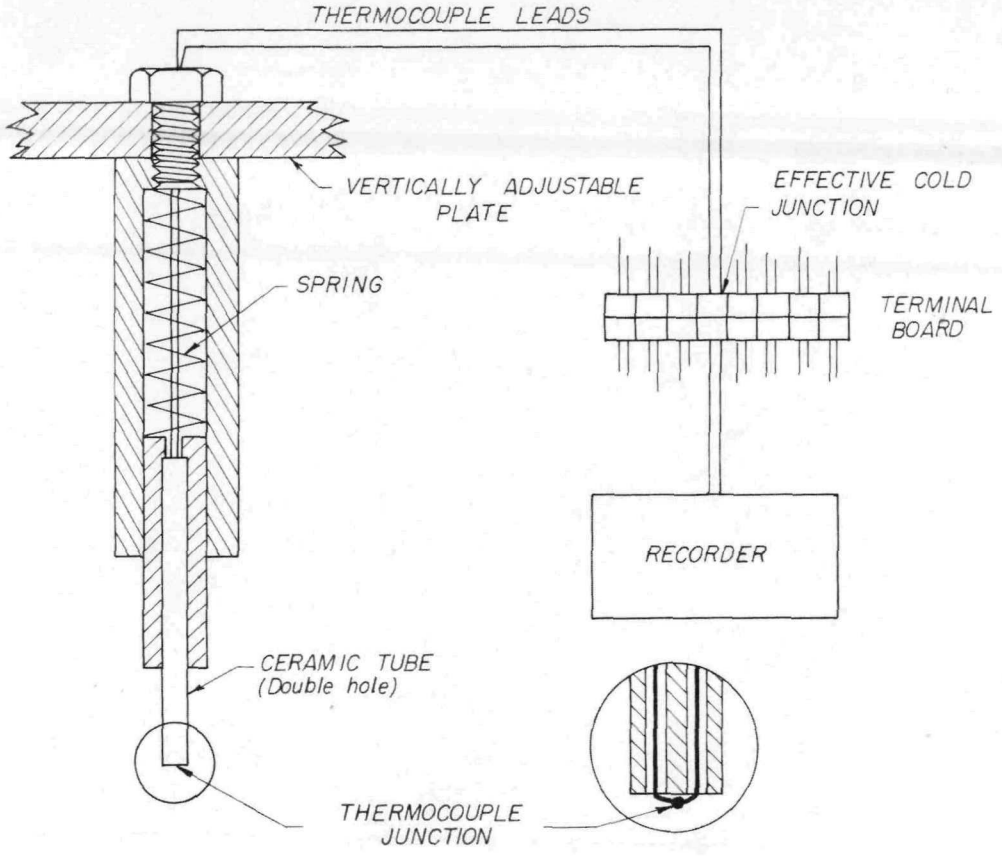

FIGURE 10a. - SCHEMATIC OF THERMOCOUPLE HOLDING DEVICE AND CIRCUIT

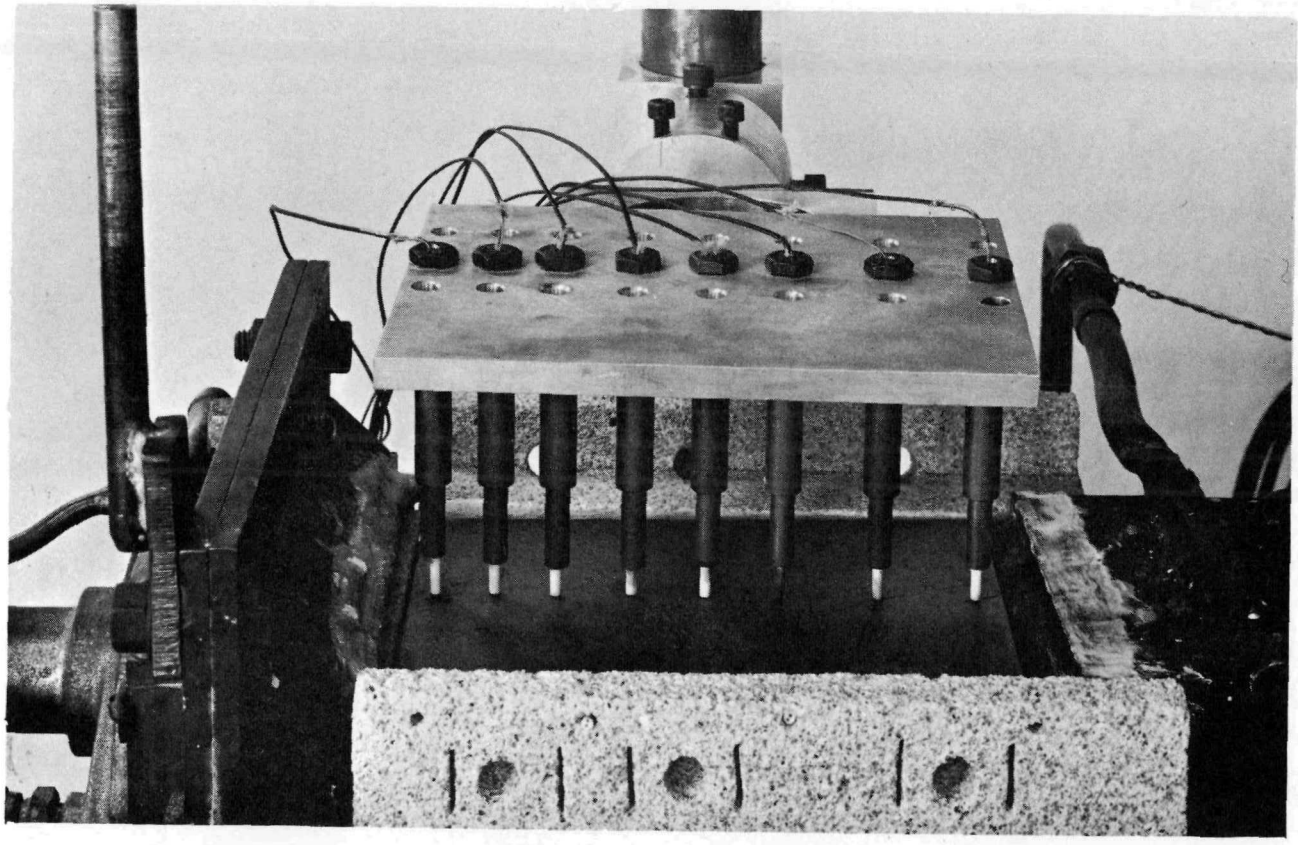

FIGURE 10b - TEMPERATURE MEASUREMENT SYSTEM

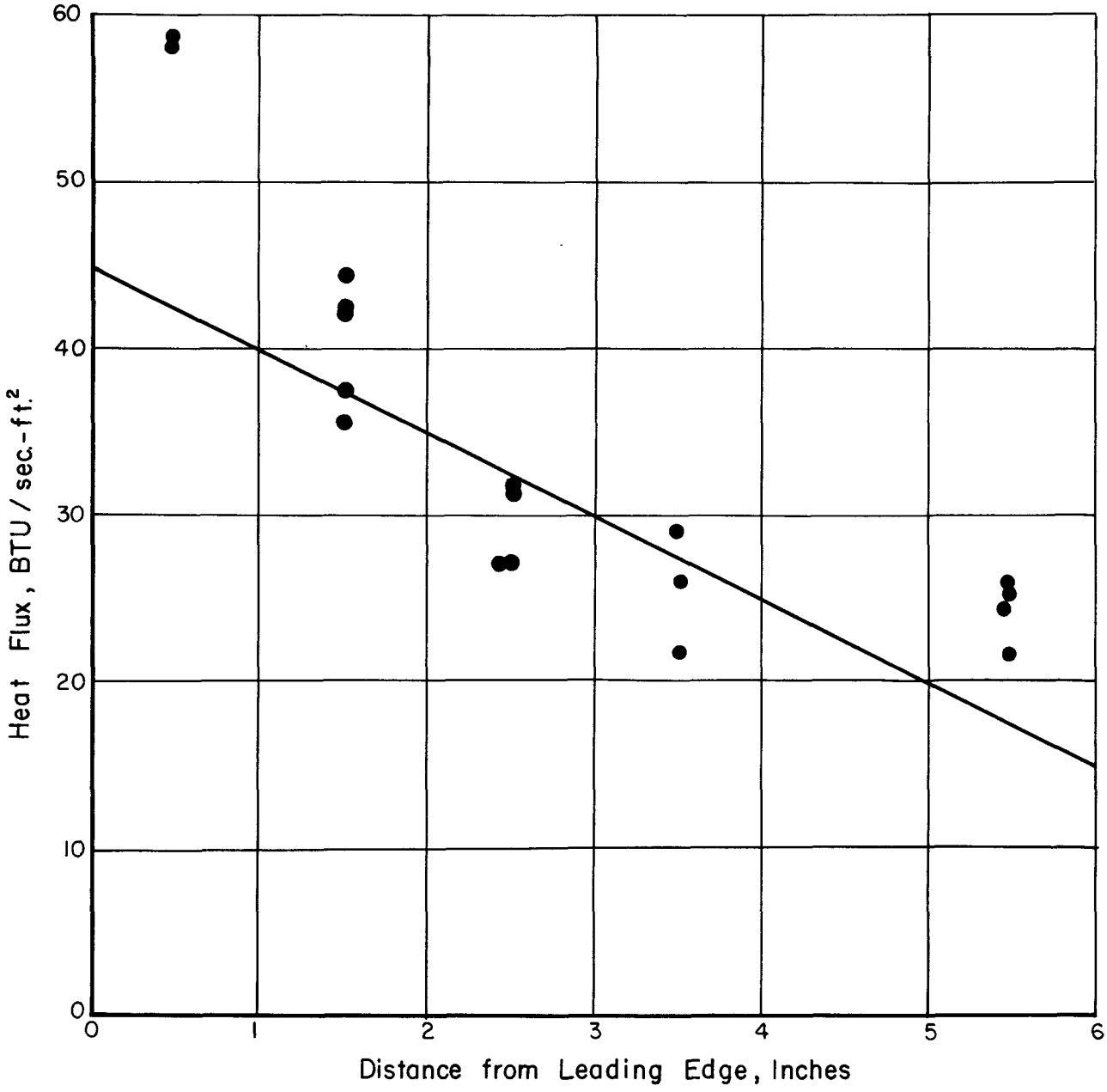

FIGURE II - HEAT FLUX DISTRIBUTION ALONG PLATE (REF. 5)

$V_{surf.}$ = 1200° R

● Experimental

—— Assumed Linear Approximation

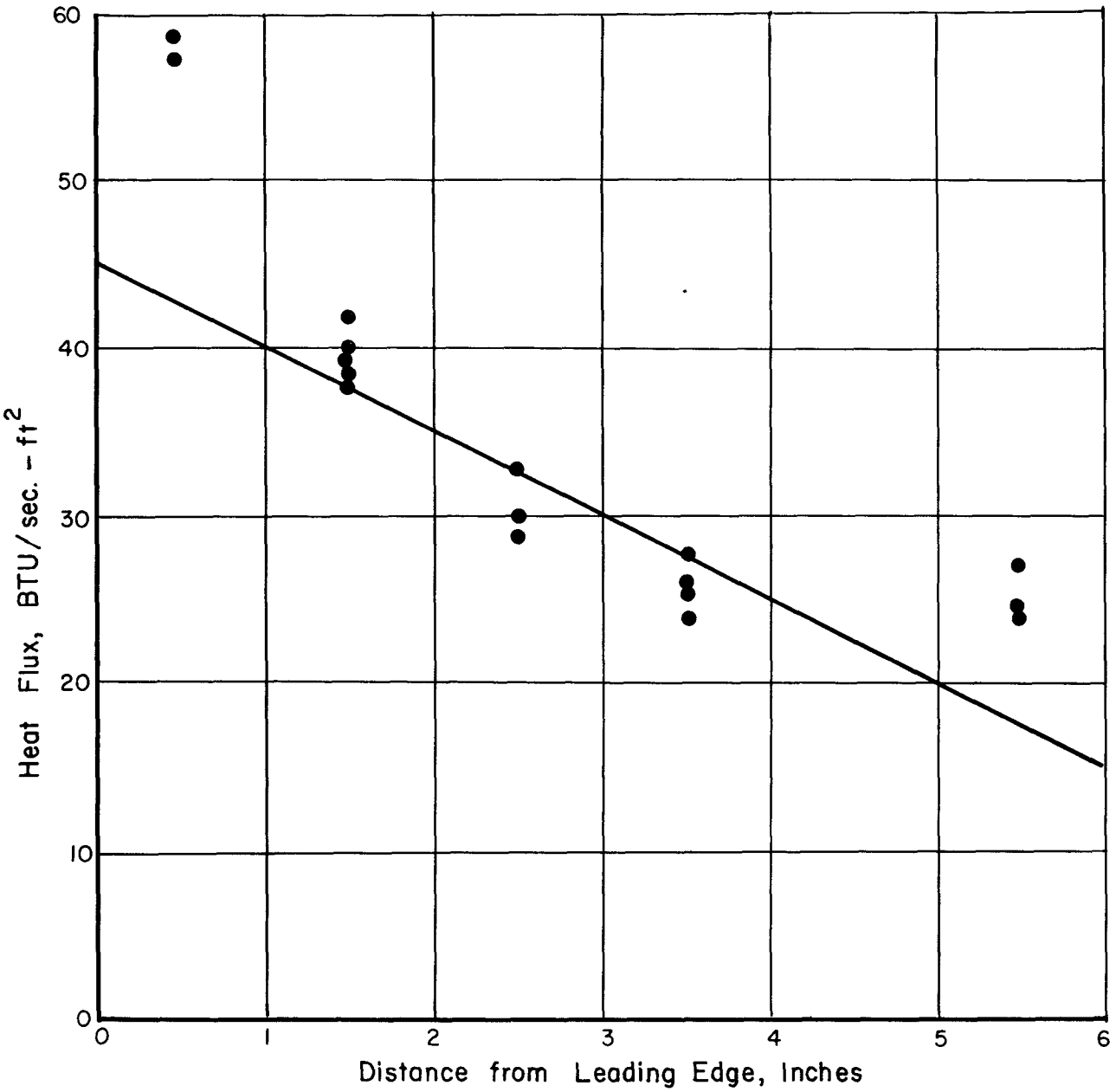

FIGURE 12 - HEAT FLUX DISTRIBUTION ALONG PLATE (REF. 5)

$V_{surf.}$ = 1600° R

● Experimental

—— Assumed Linear Approximation

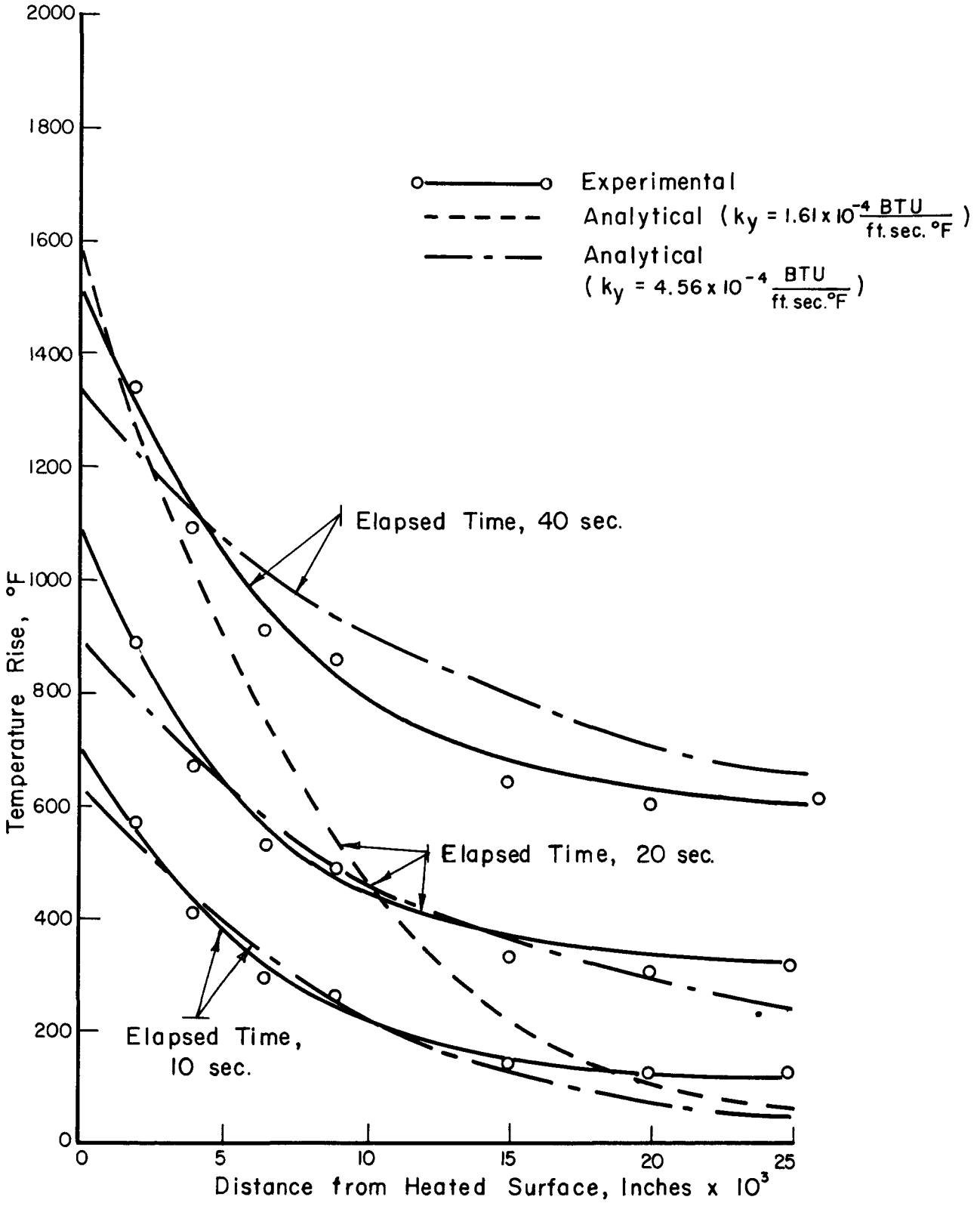

FIGURE 13 – PREDICTED AND EXPERIMENTAL TEMPERATURE DISTRIBUTIONS THROUGH A PYROLYTIC GRAPHITE PLATE 3 INCHES FROM THE LEADING EDGE

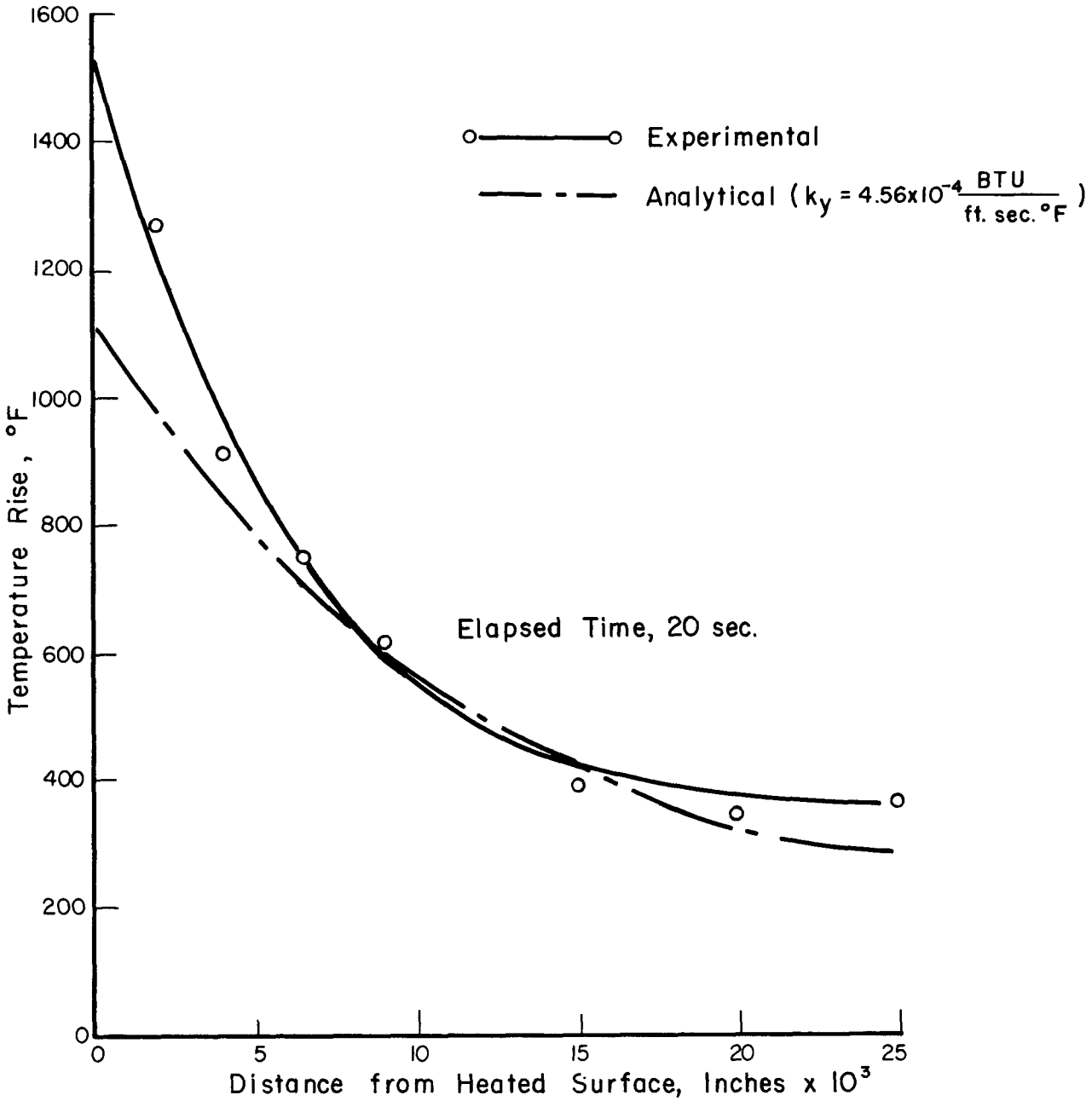

FIGURE 14 - PREDICTED AND EXPERIMENTAL TEMPERATURE DISTRIBUTIONS THROUGH A PYROLYTIC GRAPHITE PLATE $^{7}/_{8}$" FROM LEADING EDGE

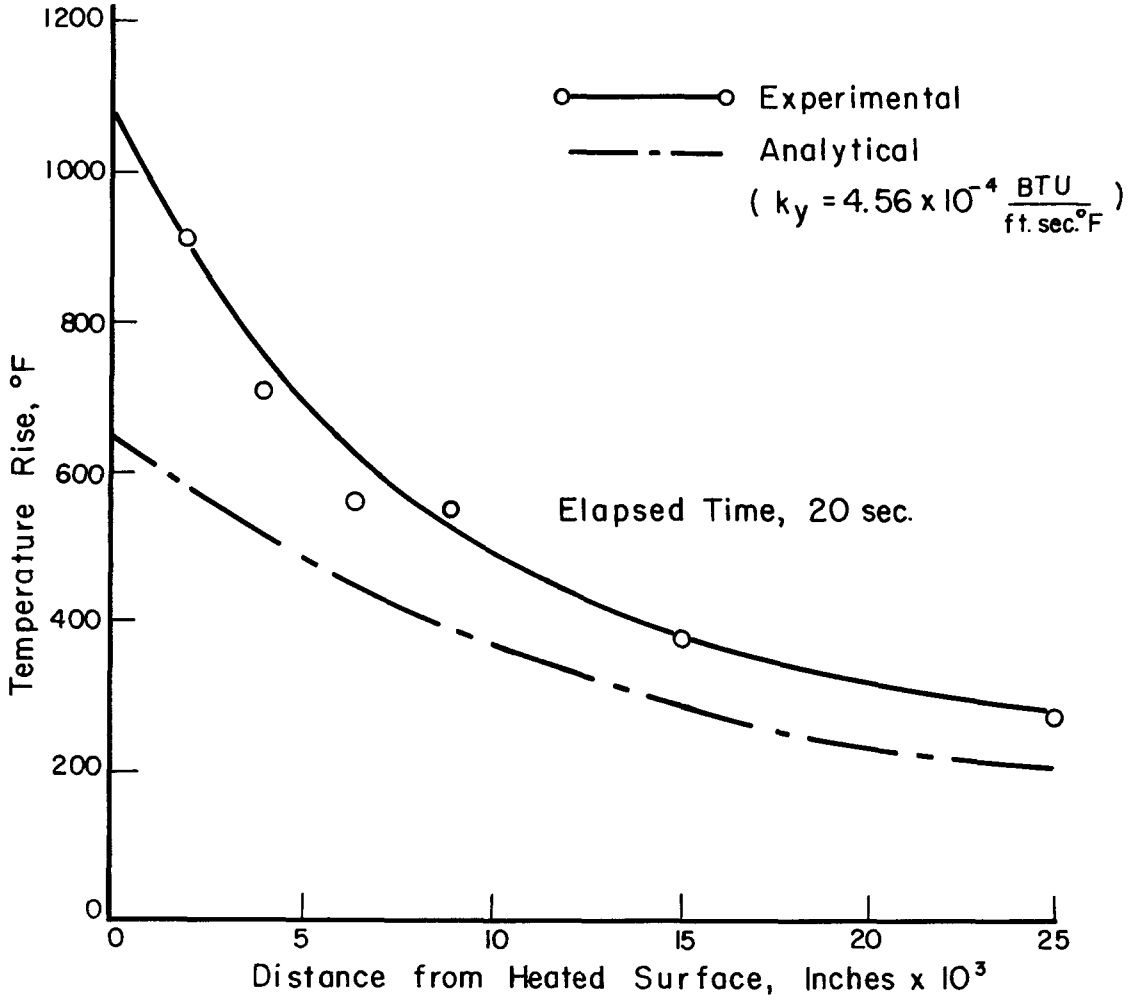

FIGURE 15 - PREDICTED AND EXPERIMENTAL TEMPERATURE DISTRIBUTIONS THROUGH A PYROLYTIC GRAPHITE PLATE 5 3/4" FROM THE LEADING EDGE

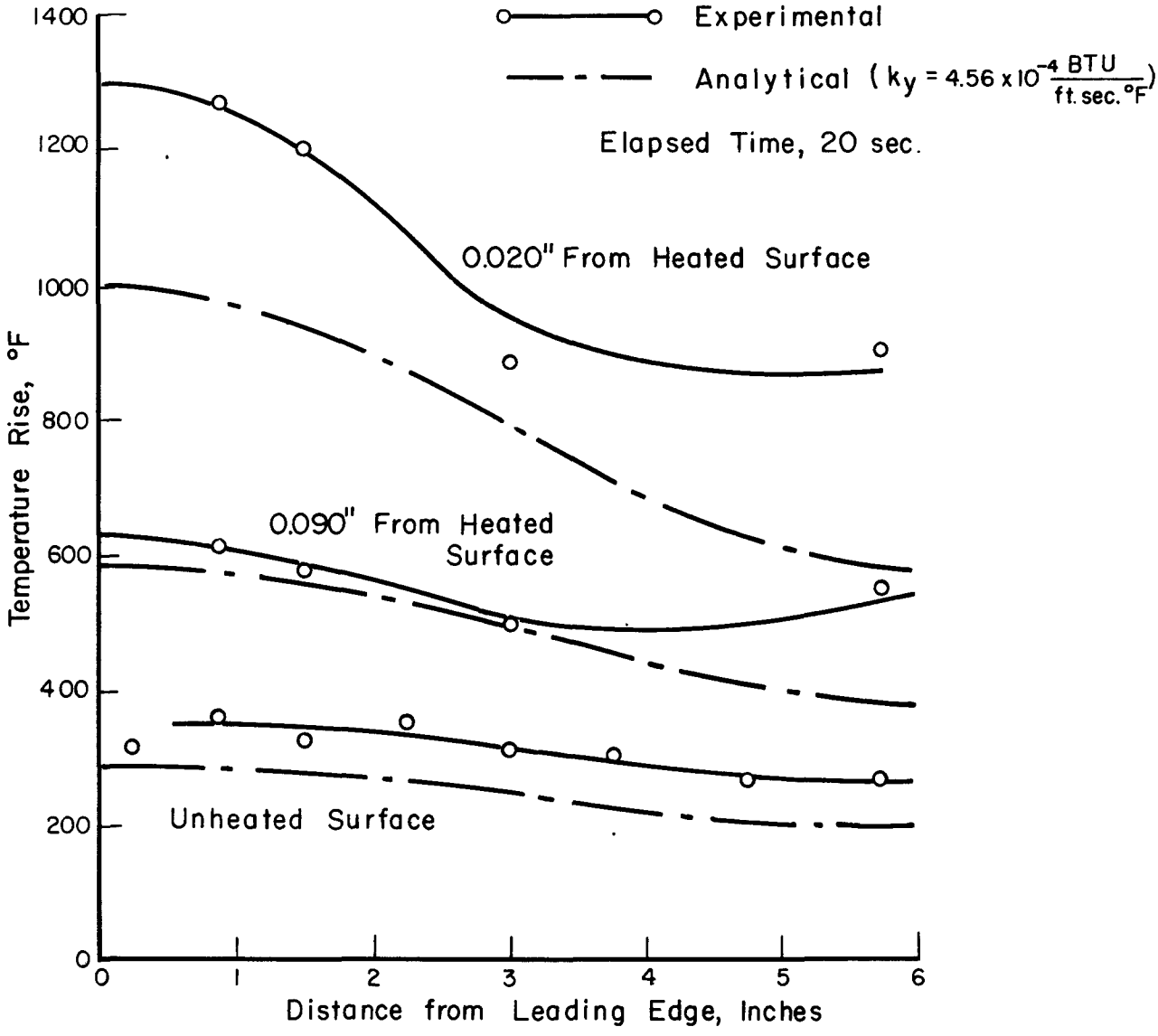

FIGURE 16 - PREDICTED AND EXPERIMENTAL TEMPERATURE DISTRIBUTIONS ALONG A PYROLYTIC GRAPHITE PLATE

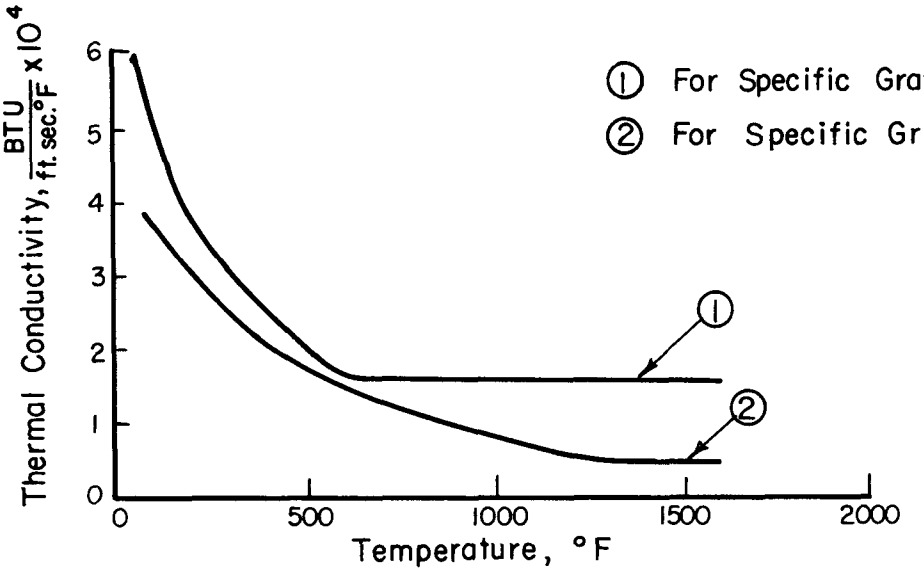

Thermal Conductivity Normal to Heated Surface (k_y)

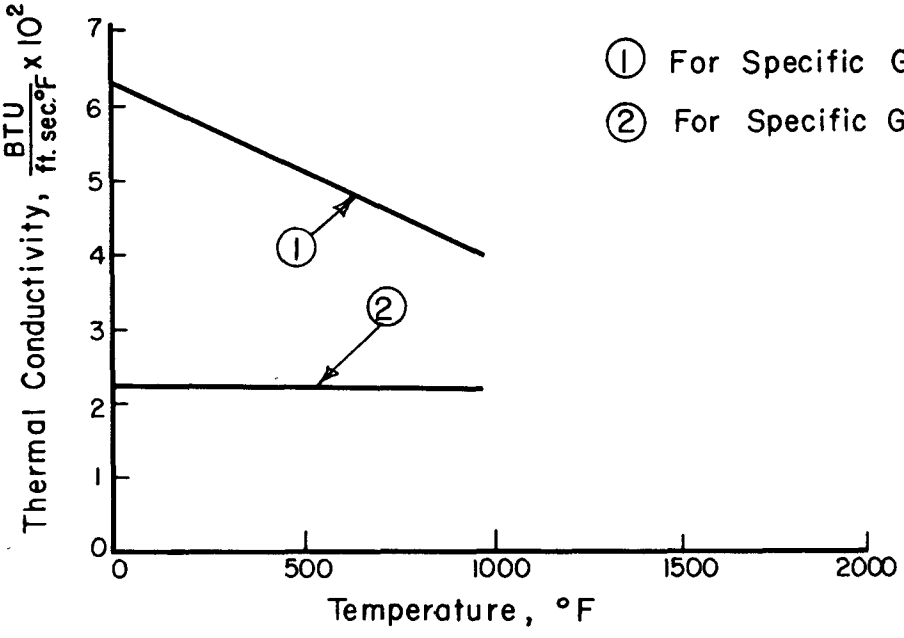

Thermal Conductivity Parallel to Heated Surface (k_x)

FIGURE 17 - THERMAL CONDUCTIVITY OF PYROLYTIC GRAPHITE VS TEMPERATURE (ref. 7)

IX. CONCLUSIONS AND RECOMMENDATIONS

1. A solution has been obtained for the transient temperature variation in a thermally orthotropic plate which is exposed to an arbitrary non-uniform heating rate distributions on one surface with all other surfaces being insulated. This solution has been used to prepare dimensionless temperature distribution curves for the case of a linearly varying heat flux. The results show both qualitatively and quantitatively the effects of the degree of orthotropy.
2. On the basis of the analysis carried out it appears that most cases of non-uniform heating rate distributions encountered in practical applications could be approximated by a linear variation, in that only small errors in the predicted temperature on the unheated surface would result. If this approximation is made, the desired temperatures may be obtained from the dimensionless curves presented.
3. Comparison of experimental measurements and analytical predictions show that the mean thermal properties of pyrolytic graphite presently available are not valid for the specimen tested. Values of thermal conductivity approximately three times those expected were required to give reasonable agreement.
4. This comparison also shows that the validity of the predicted temperatures is dependent upon the degree to which the thermal properties are dependent upon temperature.
5. It has been shown, both analytically and experimentally, that pyrolytic graphite, as representative of highly orthotropic materials, possesses an effective ability to distribute energy transferred

during non-uniform surface heating. This distributing ability results in temperatures on the unheated surface which are relatively independent of local heating but rather dependent on total heat input.

6. It is recommended that the thermal properties of the pyrolytic graphite plate used for temperature measurements be determined in order to permit a more precise comparison of the experimental and theoretical predictions.

REFERENCES

1. H. S. Carslaw, J. C. Jaegar — Conduction of Heat in Solids, Oxford University Press, 2nd Ed., London, 1959, p. 112.
2. R. V. Churchill — Operational Mathematics, McGraw Hill Book Company, New York, 2nd Ed., 1958, p. 328.
3. I. S. Sokolnikoff, R. M. Redheffer — Mathematics of Physics and Modern Engineering, McGraw Hill Book Company, New York, 1958, p. 175.
4. D. Wizansky, E. J. Russ, W. H. Giedt — "An Oxyacetylene Flame Apparatus for Surface Ablation Studies," University of California Engineering Project Report HE-150-167, January 1959.
5. L. L. Cobb, Jr. — "The Influence of Hydrogen Recombination on Turbulent Flow Heat Transfer to a Flat Plate," University of California Engineering Project Report HE-150-183, June 1960.
6. R. B. Kinney — "Ablation of Clear and Filled Teflon at Low Heating Rates," University of California Engineering Project Report HE-150-185, January 1961.
7. "Pyrolytic Graphite Data Book", Lockheed Aircraft Corporation, Missiles and Space Division, LMSD-288186, March 1960.
8. L. Lees — "Laminar Heat Transfer Over Blunt-Nosed Bodies at Hypersonic Flight Speeds," Jet Propulsion, 26, 4, 259, 1956.
9. W. H. Giedt — Principles of Engineering Heat Transfer, Van Nostrand, Princeton, N. J., 1957, p. 170.

APPENDIX A

SOLUTION PROCEDURE FOR DETERMINING TRANSIENT TEMPERATURES IN A THERMALLY ORTHOTROPIC PLATE

The system to be considered is sketched in Figure 1. In obtaining an expression for the transient temperatures in such a system, the time dependent two-dimensional heat conduction equation with orthotropic thermal properties is applicable. This equation is:

$$\frac{\partial v}{\partial t} = \alpha_{x'} \frac{\partial^2 v}{\partial x'^2} + \alpha_{y'} \frac{\partial^2 v}{\partial y'^2} \tag{1}$$

subject to the following boundary and initial conditions:

$$\frac{\partial v}{\partial x'} = 0 \qquad \text{at } x' = 0,\ x' = \ell' \qquad 0 \le y' \le a' \tag{1-a}$$

$$\frac{\partial v}{\partial y'} = 0 \qquad \text{at } y' = 0 \qquad 0 \le x' \le \ell' \tag{1-b}$$

$$-k_{y'} \frac{\partial v}{\partial y'} = f(x') \quad \text{at } y' = a' \qquad 0 \le x' \le \ell' \tag{1-c}$$

$$v = 0 \qquad \text{at } t = 0 \qquad \begin{matrix} 0 \le y' \le a' \\ 0 \le x' \le \ell' \end{matrix} \tag{1-d}$$

The problem is first reduced to the isotropic case by the following change of variables:

$$x = \frac{x'}{\sqrt{\alpha_{x'}}}, \quad y = \frac{y'}{\sqrt{\alpha_{y'}}}, \quad \ell = \frac{\ell'}{\sqrt{\alpha_{x'}}}, \quad a = \frac{a'}{\sqrt{\alpha_{y'}}}$$

This results in:

$$\frac{\partial v}{\partial t} = \frac{\partial^2 v}{\partial x^2} + \frac{\partial^2 v}{\partial y^2} \tag{A-1}$$

$$\frac{\partial v}{\partial x} = 0 \qquad \text{at } x = 0,\ x = \ell \qquad 0 \le y \le a \tag{A-1-a}$$

$$\frac{\partial v}{\partial y} = 0 \qquad \text{at } y = 0 \qquad 0 \le x \le \ell \qquad \text{(A-1-b)}$$

$$\frac{\partial v}{\partial y} = \frac{\sqrt{\alpha_{y'}}}{k_{y'}} f(x\sqrt{\alpha_{x'}}) = g(x) \text{ at } y = a \qquad 0 \le x \le \ell \qquad \text{(A-1-c)}$$

$$v = 0 \quad \text{at} \quad t = 0 \qquad \begin{matrix} 0 \le y \le a \\ 0 \le x \le \ell \end{matrix} \qquad \text{(A-1-d)}$$

The independent variables involved, (t,x,y), are now reduced to (x,y) by the use of the Laplace transformation defined by:

$$\mathcal{L}\, v(t,x,y) = \bar{v}(s,x,y) = \int_0^\infty v(t,x,y)e^{-st}\, dt$$

The differential equation becomes

$$s\bar{v} = \frac{\partial^2 \bar{v}}{\partial x^2} + \frac{\partial^2 \bar{v}}{\partial y^2} \qquad (2)$$

and the boundary conditions:

$$\frac{\partial \bar{v}}{\partial x} = 0 \qquad \text{at } x = 0, \quad x = \ell \qquad \text{(2-a)}$$

$$\frac{\partial \bar{v}}{\partial y} \qquad \text{at } y = 0 \qquad \text{(2-b)}$$

$$\frac{\partial \bar{v}}{\partial y} = \frac{g(x)}{s} \qquad \text{at } y = a \qquad \text{(2-c)}$$

In the solution of this equation s is treated as a constant.

The method of separation of variables may now be employed. Assuming $\bar{v}(s,x,y) = X(x)\,Y(y)$ and substituting this assumed form of the solution into equation (2), separating variables results in the following:

$$X'' + \beta^2 X = 0 \qquad \text{(A-2)}$$

$$Y'' - (\beta^2 + s)Y = 0 \qquad \text{(A-3)}$$

where primes indicate differentiation with respect to the corresponding variable and β^2 is a separation constant.

Solutions to equations (A-2) and (A-3) which satisfy the boundary conditions (2-a) and (2-b) are:

$$X = C_1 \cos \beta x \tag{A-4}$$

$$Y = C_2 \cosh y\sqrt{\beta^2 + s} \qquad \text{where} \quad \beta = \frac{n\pi}{\ell} \tag{A-5}$$

Combining equations (A-4) and (A-5) and summing over all β to obtain the general solution yields:

$$\overline{v}(s,x,y) = \sum_{n=0}^{\infty} C_n \cos \beta x \cosh y\sqrt{\beta^2 + s} \tag{A-6}$$

C_n may be determined from the boundary condition, $\frac{\partial \overline{v}}{\partial y} = \frac{g(x)}{s}$ at $y = a$. This gives

$$\overline{v}(s,x,y) = \sum_{n=0}^{\infty} \frac{A_n \cos \beta x \cosh y\sqrt{\beta^2 + s}}{s\sqrt{\beta^2 + s} \sinh a\sqrt{\beta^2 + s}} \tag{A-7}$$

where $g(x) = \sum_{n=0}^{\infty} A_n \cos \frac{n\pi x}{\ell}$.

This solution can be shown to satisfy equations (2).

The inversion of equation (A-7) to the real time domain was accomplished term by term. A typical term of interest is, letting $(\beta^2 + s)^{1/2} = m$:

$$\frac{\cosh my}{sm \sinh ma} = P_n \tag{A-8}$$

then

$$P_n = \frac{e^{my} + e^{-my}}{sm\,[e^{ma} - e^{-ma}]} \tag{A-9}$$

It may be shown that for $|e^{-2ma}| < 1$

$$P_n = \frac{e^{-m(a-y)} + e^{-m(a+y)}}{sm} \sum_{i=0}^{\infty} e^{-2ima} \qquad \text{(A-10)}$$

Apparently the restrictions placed here on s have no effect on the solution as the resulting expression satisfies the original differential equation.

Rearranging,

$$P_n = \sum_{i=0}^{\infty} \left(\frac{1}{sm}\right)\left(e^{-mb_1} + e^{-mb_2}\right) \qquad \text{(A-11)}$$

where $b_1 = [(2i + 1)a-y]$

$b_2 = [(2i + 1)a+y]$

This series was also inverted termwise.

The following inversion principle is now noted:

$$\mathcal{L}^{-1} \left\{ \frac{1}{s} f(s)\right\} = \int_o^t f(t)\ dt \qquad \text{(A-12)}$$

With this in mind, consider the term,

$$\frac{e^{-mb}}{m} = \frac{e^{-(\beta^2 + s)^{1/2}b}}{\sqrt{\beta^2 + s}} \qquad \text{(A-13)}$$

The shifting theorem in Laplace transform theory is

$$\mathcal{L}^{-1} \left\{f(s + a)\right\} = e^{-at} f(t)$$

Equation (A-13) is of this form where $a = \beta^2$.

The function to be inverted is therefore

$$\frac{e^{-\sqrt{s}\ b}}{\sqrt{s}}$$

From a table of transforms, (e.g., reference 2),

$$\mathcal{L}^{-1}\left\{\frac{e^{-b\sqrt{s}}}{\sqrt{s}}\right\} = \frac{1}{\sqrt{\pi\ t}}\quad e^{-\frac{b^2}{4t}} \tag{A-14}$$

Thus:

$$\mathcal{L}^{-1}\quad\left\{\frac{e^{-(\beta^2+s)^{1/2}\ b}}{\sqrt{\beta^2+s}}\right\} = \frac{e^{-\beta^2 t}}{\sqrt{\pi\ t}}\quad e^{-\frac{b^2}{4t}} \tag{A-15}$$

Recalling the significance of $1/s$ from equation (A-12) and applying the above result gives

$$v(t,x,y) = \sum_{n=0}^{\infty}\ \sum_{i=0}^{\infty} A_n \cos\beta x \int_o^t \frac{\exp(-\beta^2 t)}{\sqrt{\pi\ t}}\left[\exp\left(-\frac{b_1^2}{4t}\right) + \exp\left(-\frac{b_2^2}{4t}\right)\right] dt \tag{A-16}$$

Equation (A-16) is the complete solution in terms of the transformed variables x and y but is not in a desirable form for numerical evaluation. In order to make the expression usable for computations the integration must be performed.

The typical term which must be integrated is

$$\int_o^t \frac{1}{\sqrt{\pi\ t}}\quad \exp\left[-\left(\beta^2 t + \frac{b^2}{4t}\right)\right] dt \tag{A-17}$$

Letting $\mu = \frac{b}{2}$ and $\lambda = \beta\sqrt{t}$,

$$t = \frac{\lambda^2}{\beta^2}$$

It can be seen that this step is valid only if $\beta \neq 0$. The special case of $\beta = 0$ is treated separately below.

When the above substitutions are made, equation (A-17) becomes:

$$\frac{2}{\beta\sqrt{\pi}} \int_{o}^{\beta\sqrt{t}} \exp\left[-\left(\lambda^2 + \frac{\mu^2\beta^2}{\lambda^2}\right)\right] d\lambda \qquad \text{(A-18)}$$

The exponent can be rearranged to be $\left[-\left(\lambda - \frac{\mu\beta}{\lambda}\right)^2 - 2\mu\beta\right]$ and a new variable $\xi = \left(\lambda - \frac{\mu\beta}{\lambda}\right)$ defined. Substitution of ξ into equation (A-18) gives:

$$\frac{\exp(-2\mu\beta)}{\beta\sqrt{\pi}}\left[\int_{-\infty}^{\left[\beta\sqrt{t} - \frac{\mu}{\sqrt{t}}\right]} e^{-\xi^2} d\xi + \int_{-\infty}^{\left[\beta\sqrt{t} - \frac{\mu}{\sqrt{t}}\right]} \frac{\xi\, e^{-\xi^2}}{\sqrt{\xi^2 + 4\mu\beta}} d\xi\right] \qquad \text{(A-19)}$$

The first integral in equation (A-19) is of the error function type and can be shown to be equal to $\frac{\sqrt{\pi}}{2}(1 + \text{erf } \xi)$.

The second integral in equation (A-19) can be evaluated by substituting $\eta = \sqrt{\xi^2 + 4\mu\beta}$. Integration then yields $-\frac{\sqrt{\pi}}{2}\exp(4\mu\beta)\ \text{erfc}\ \eta$.

Combining these results, equation (A-19) becomes

$$\frac{\exp(-2\mu\beta)}{2\beta}(1 + \text{erf } \xi) - \frac{\exp(2\mu\beta)}{2\beta}\ \text{erfc}\ \eta\ . \qquad \text{(A-20)}$$

For the case of $\beta = 0$, equation (A-17) takes the form

$$\int_{o}^{t} \frac{1}{\sqrt{\pi\, t}} \exp\left(-\frac{b^2}{4t}\right) dt \qquad \text{(A-21)}$$

Substituting $\omega = \frac{b}{2\sqrt{t}}$ and integrating by parts, equation (A-21) becomes

$$\frac{2\sqrt{t}}{\sqrt{\pi}} \exp\left(-\frac{b^2}{4t}\right) - b\ \text{erfc}\left(\frac{b}{2\sqrt{t}}\right) \qquad \text{(A-22)}$$

Replacing the integral in equation (A-16) by the results obtained in equations (A-20) and (A-22), the desired expression for the temperature is:

$$v(t,x,y) = \sum_{i=0}^{\infty} A_o \left\{ \frac{2\sqrt{t}}{\sqrt{\pi}} \exp\left(-\frac{b_1^2}{4t}\right) - b_1 \operatorname{erfc}\left(\frac{b_1}{2\sqrt{t}}\right) \right.$$

$$\left. + \frac{2\sqrt{t}}{\sqrt{\pi}} \exp\left(-\frac{b_2^2}{4t}\right) - b_2 \operatorname{erfc}\left(\frac{b_2}{2\sqrt{t}}\right) \right\}$$

$$+ \sum_{n=1}^{\infty} \sum_{i=0}^{\infty} \frac{A_n \cos(\beta x)}{2\beta} \left\{ \exp(-b_1\beta) \left[1 + \operatorname{erf}\left(\beta\sqrt{t} - \frac{b_1}{2\sqrt{t}}\right) \right] \right.$$

$$- \exp(b_1\beta) \operatorname{erfc}\left(\beta\sqrt{t} + \frac{b_1}{2\sqrt{t}}\right) + \exp(-b_2\beta) \left[1 + \operatorname{erf}\left(\beta\sqrt{t} - \frac{b_2}{2\sqrt{t}}\right) \right]$$

$$\left. - \exp(b_2\beta) \operatorname{erfc}\left(\beta\sqrt{t} + \frac{b_2}{2\sqrt{t}}\right) \right\} \qquad \text{(A-23)}$$

Where: $\beta = \frac{n\pi}{\ell}$ $\qquad b_1 = [(2i + 1)a - y]$

$g(x) = \sum_{n=0}^{\infty} A_n \cos\frac{n\pi x}{\ell}$ $\qquad b_2 = [(2i + 1)a + y]$

When the definition of $g(x)$ and the real variables (x', y', a', ℓ') are substituted into equation (A-23), and primes dropped, equation (5) in Section II is obtained.

APPENDIX B

PREDICTED TEMPERATURE HISTORIES FOR LONG TIMES AT SEVERAL POINTS

The following figures are an extension of Figures 2, 3, and 4 to longer values of time and to other points (ζ,ψ). The curves for points along $\zeta = 1/2$ and $\zeta = 1$ were obtained from the corresponding curves at $\zeta = 0$ by the simple cosine relation indicated by the analytical solution and are discussed in Section V-A.

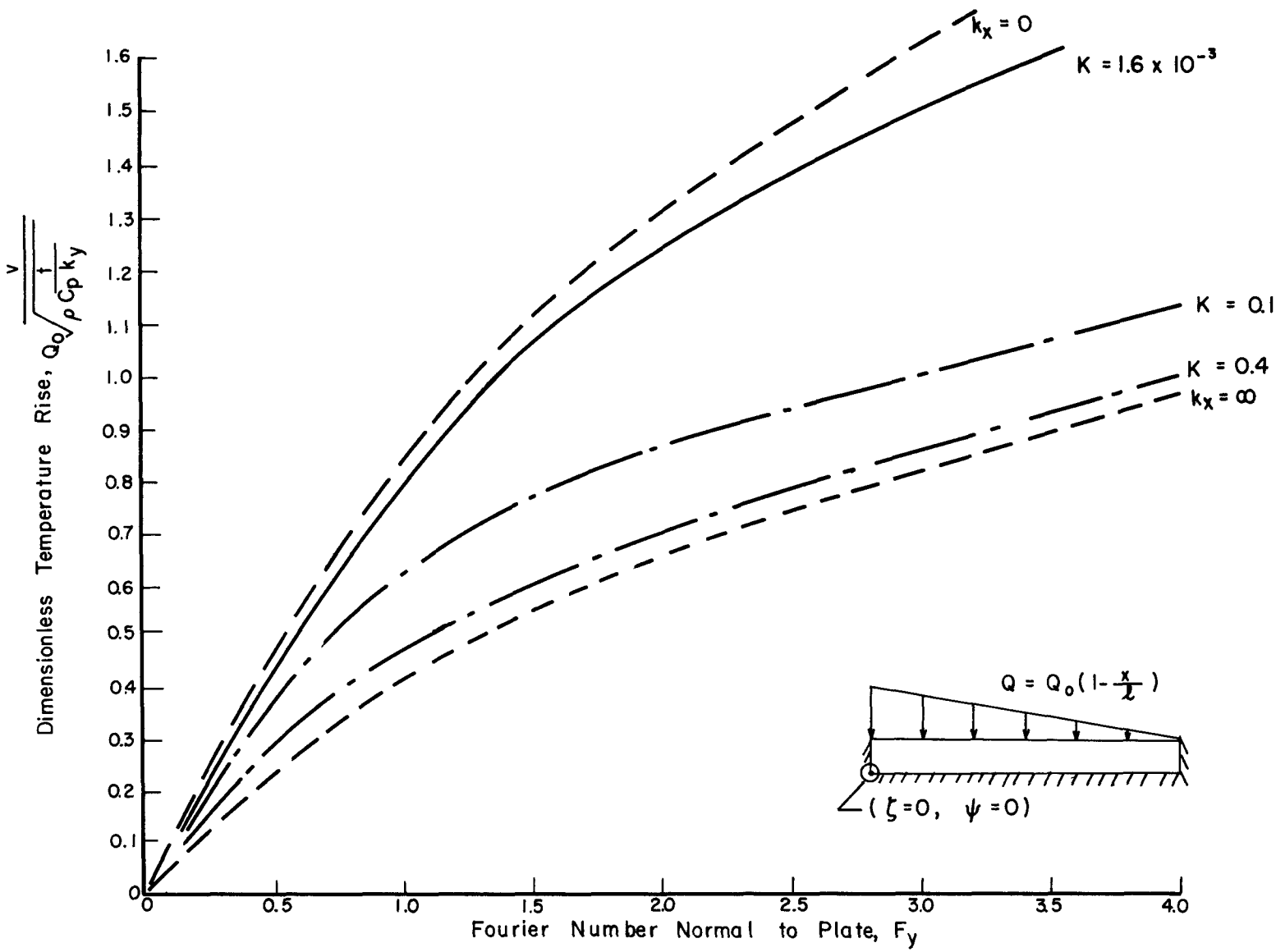

FIGURE A-1 - PREDICTED TEMPERATURE VARIATION AT LEADING EDGE OF UNHEATED SURFACE

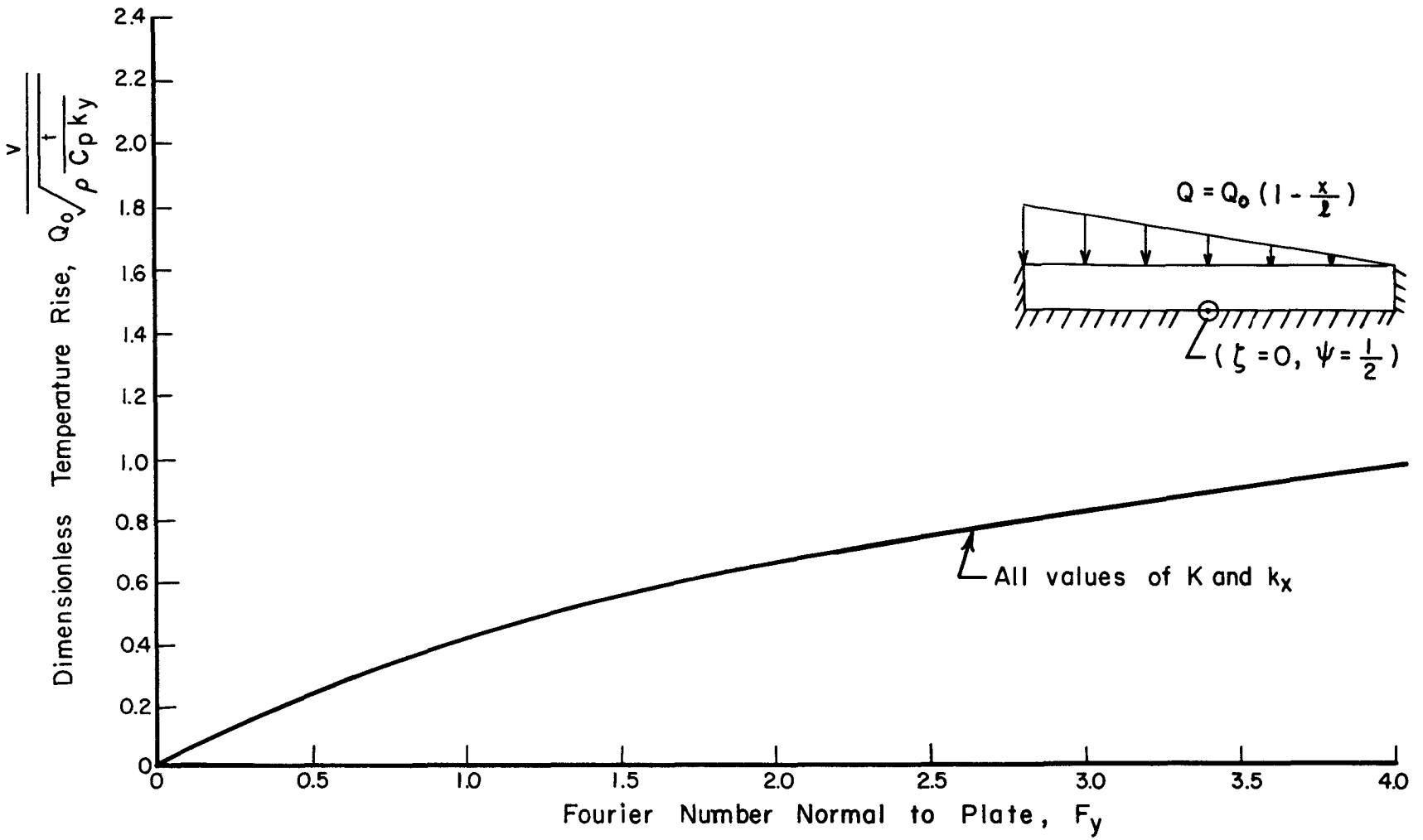

FIGURE A-2 - PREDICTED TEMPERATURE VARIATION AT MIDPOINT OF UNHEATED SURFACE

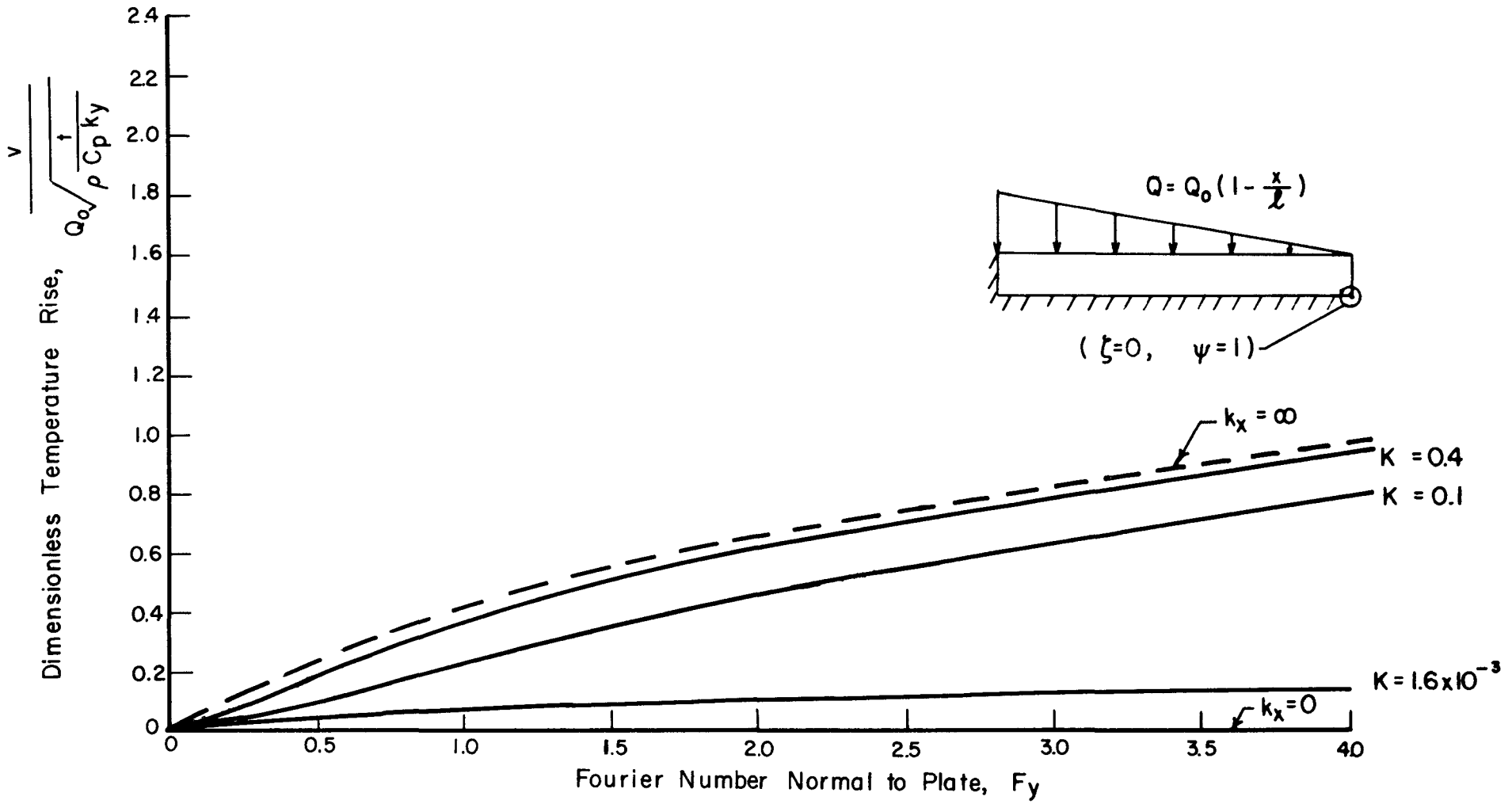

FIGURE A-3 – PREDICTED TEMPERATURE VARIATION AT TRAILING EDGE OF UNHEATED SURFACE

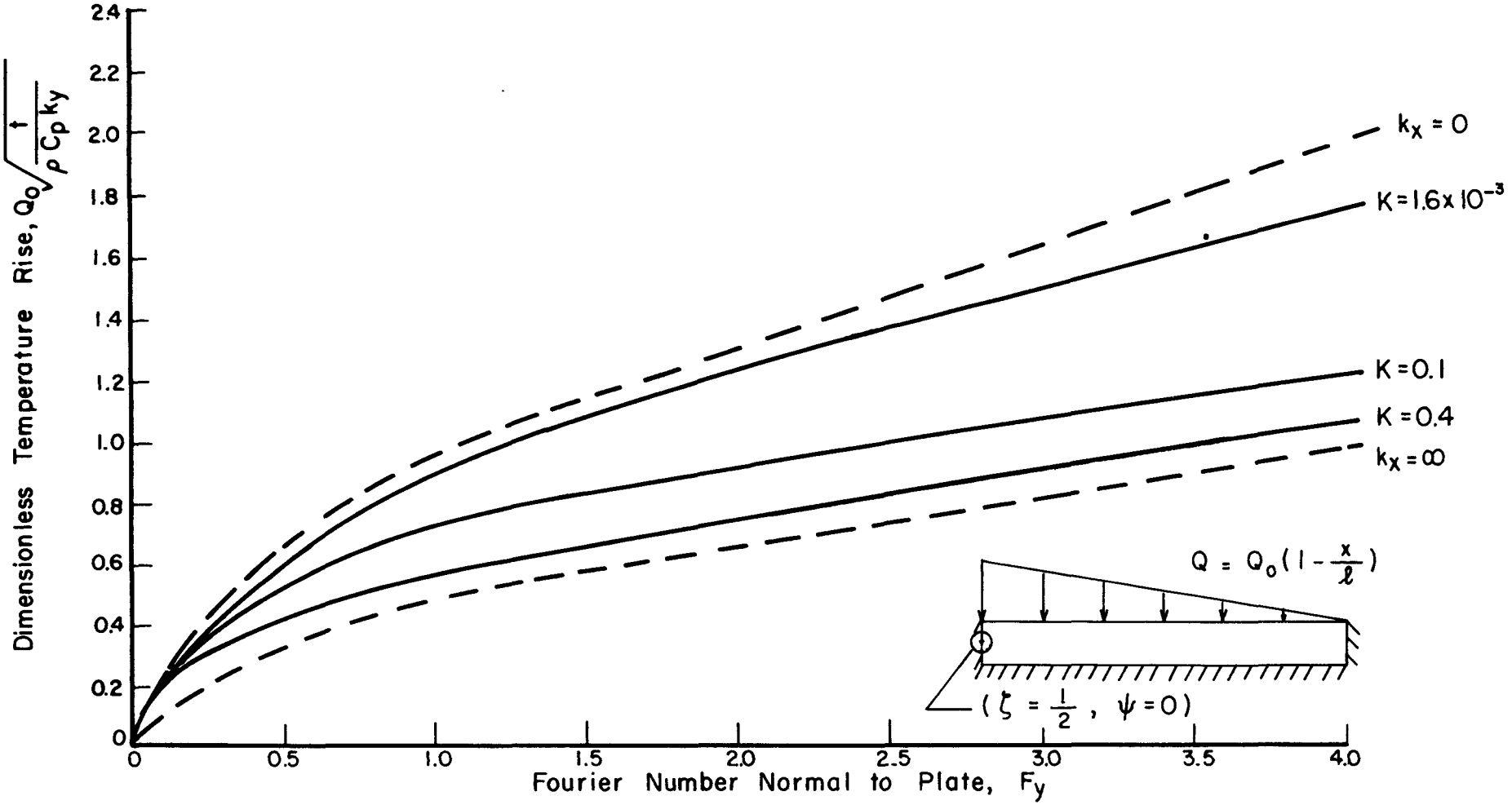

FIGURE A-4 - PREDICTED TEMPERATURE VARIATION AT LEADING EDGE OF MIDPLANE

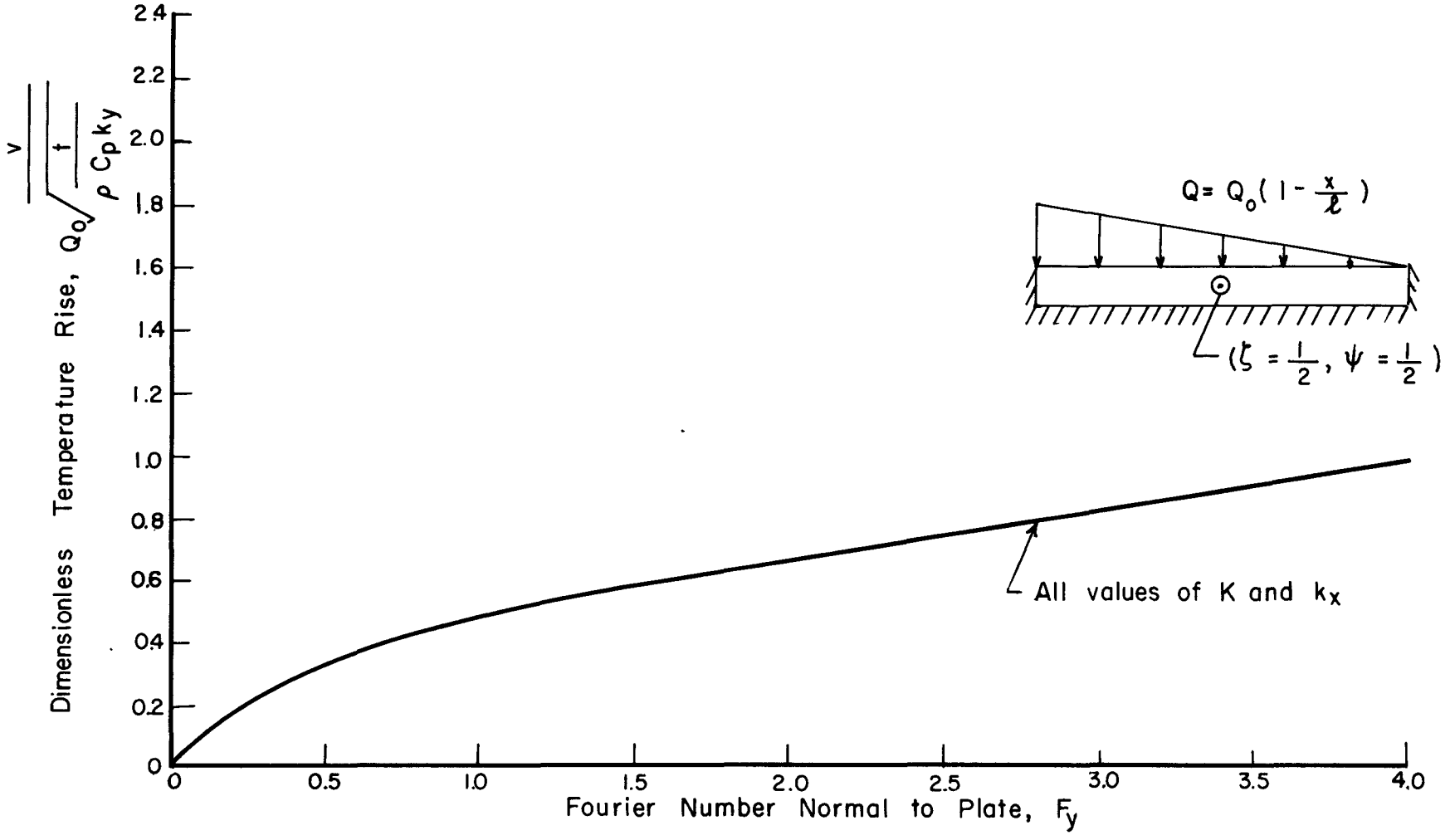

FIGURE A-5 - PREDICTED TEMPERATURE VARIATION AT MIDPOINT OF MIDPLANE

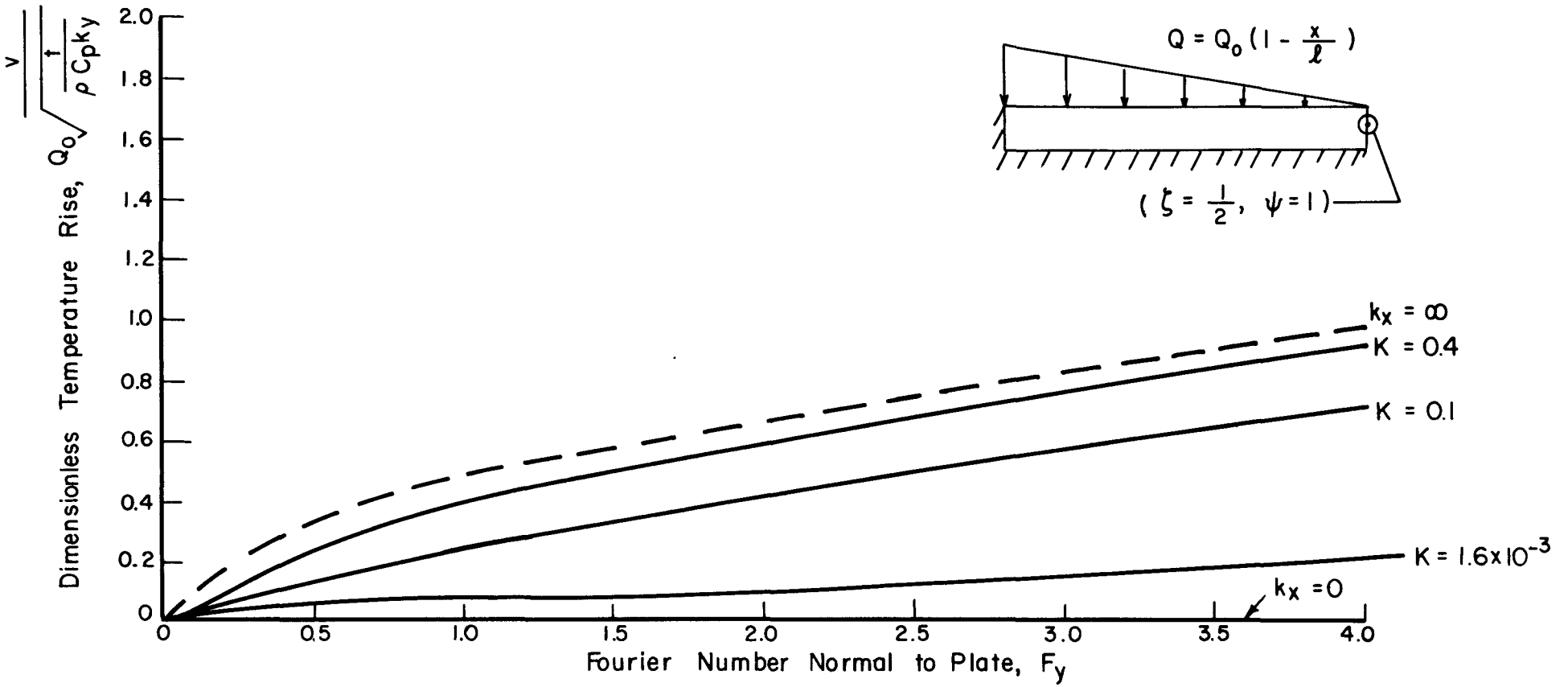

FIGURE A-6 – PREDICTED TEMPERATURE VARIATION AT TRAILING EDGE OF MIDPLANE

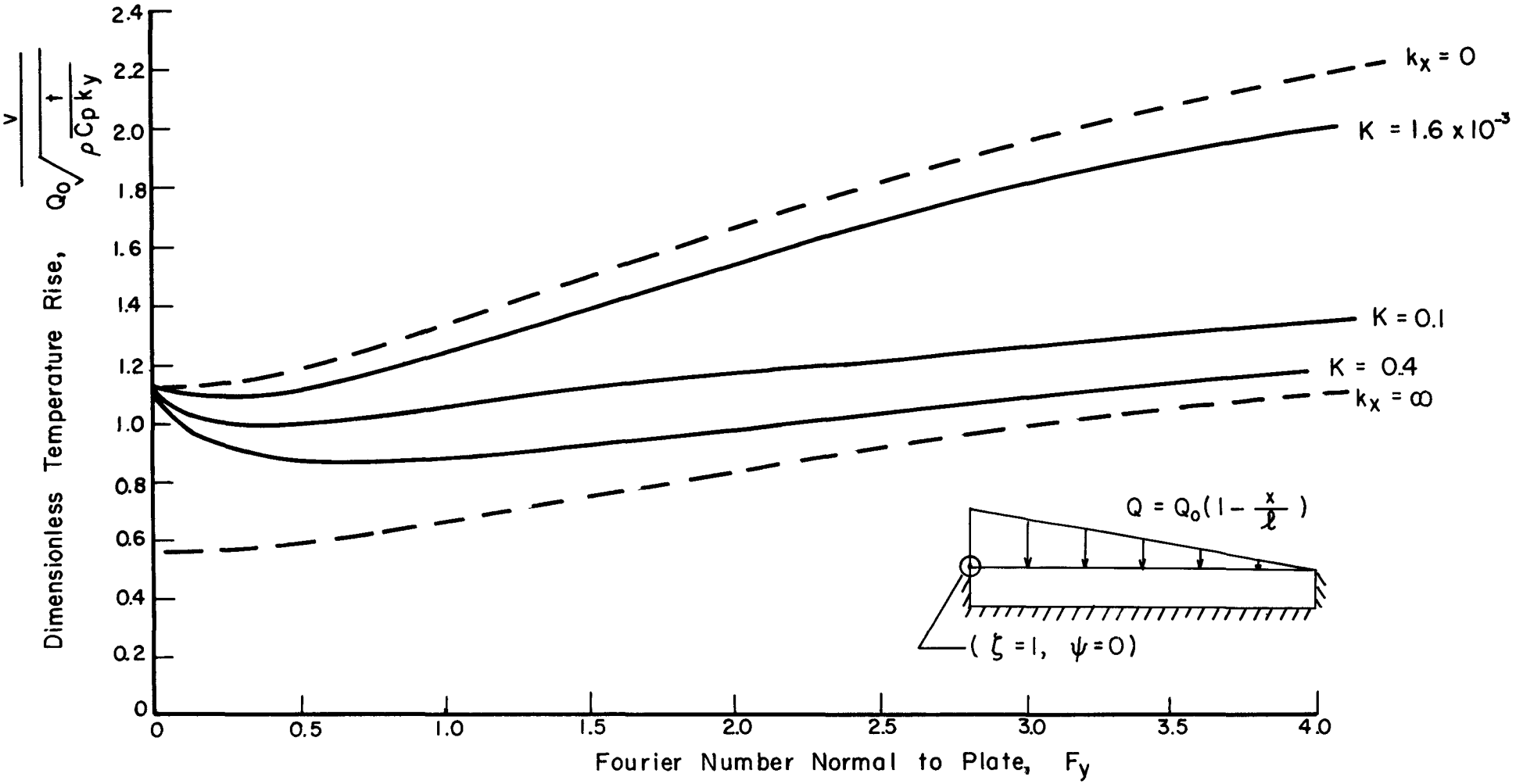

FIGURE A-7 - PREDICTED TEMPERATURE VARIATION AT LEADING EDGE OF HEATED SURFACE

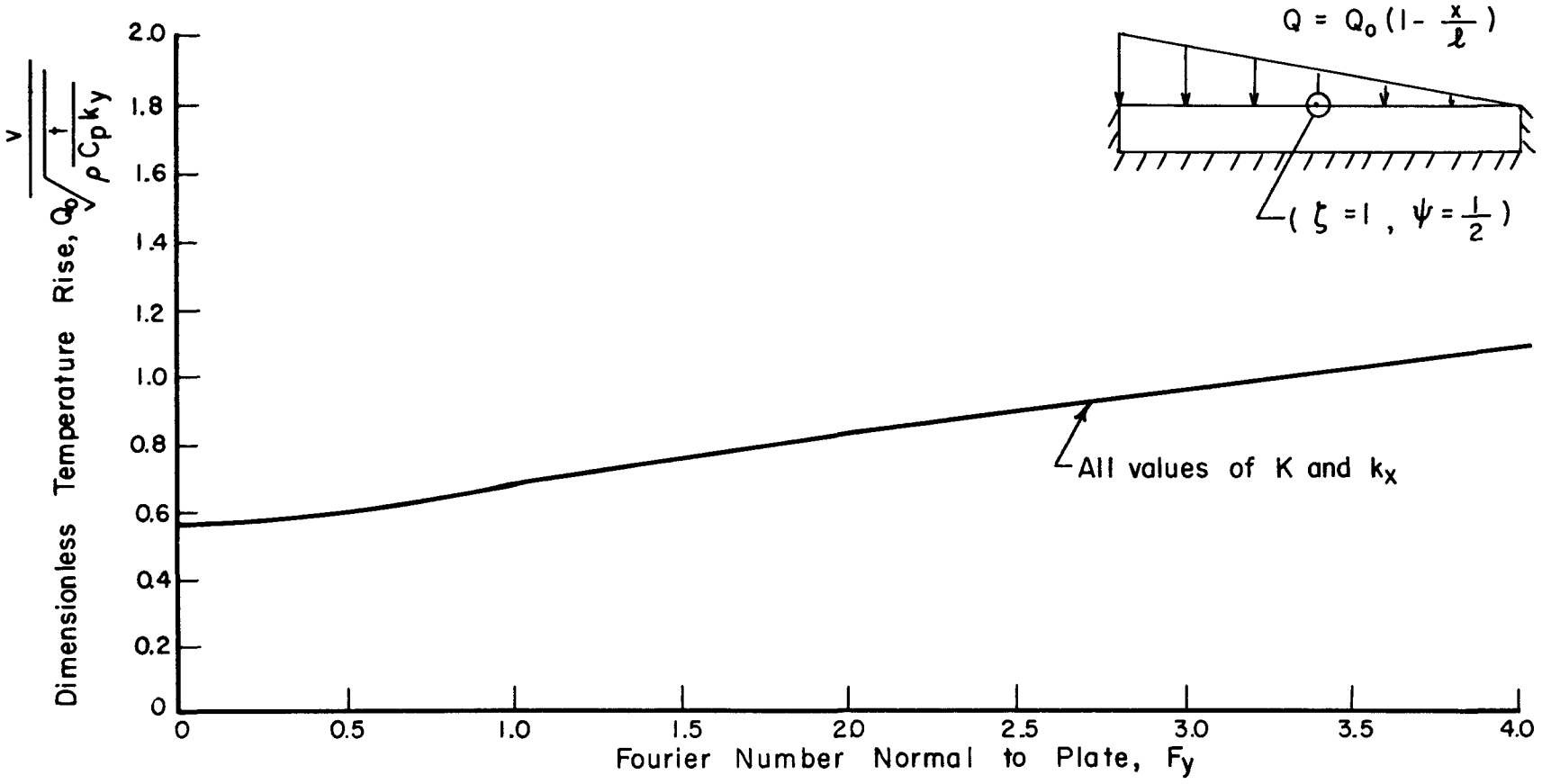

FIGURE A-8 - PREDICTED TEMPERATURE VARIATION AT MIDPOINT OF HEATED SURFACE

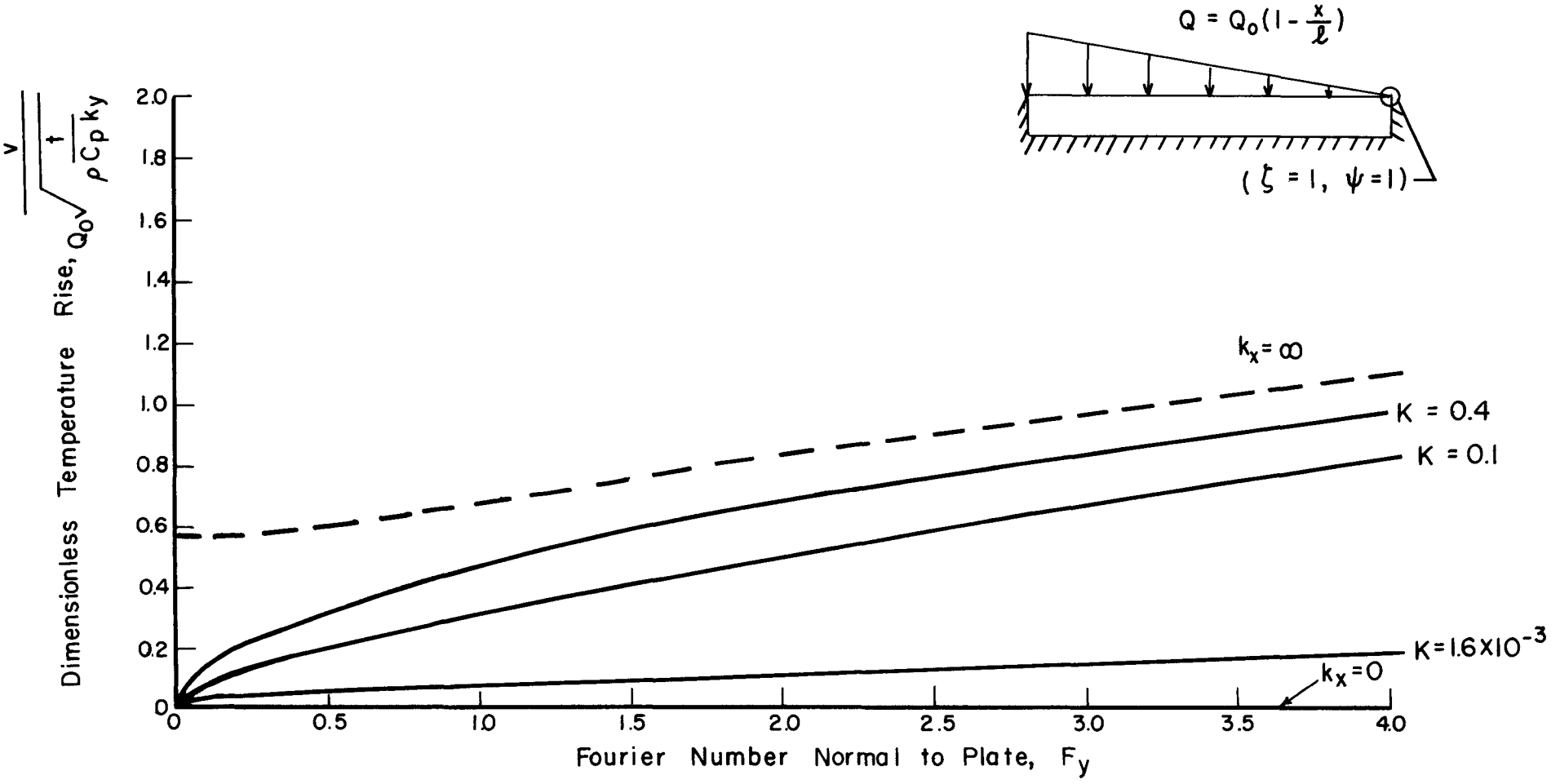

FIGURE A-9 – PREDICTED TEMPERATURE VARIATION AT TRAILING EDGE OF HEATED SURFACE

APPENDIX C

COMPARISON OF EXPERIMENTAL TEMPERATURE DISTRIBUTIONS WITH ANALYTICAL RESULTS BASED ON RECENT THERMAL CONDUCTIVITY DATA

Shortly after the completion of this study additional data on the thermal conductivity of pyrolytic graphite in the "c" direction became available. This is plotted in Fig. C-1 which includes the results of thermal conductivity measurements made by different laboratories on different samples. The wide variation evident is undoubtedly due to different manufacturing procedures and conditions.

The material used in the present investigation was obtained from High Temperature Materials, Inc. Preference should therefore be given to curves 1, 2, 5 and 8 in Fig. C-1. The average temperature during the first 20 seconds of heating was around 400 to 500 F which led to the use of a value of 4.0×10^{-4} Btu/sec ft F for k_y. The value of C_p determined from Fig. C-2. was 0.31 Btu/lb F. $k_x/k_y = 200$ was based on High Temperature Materials, Inc. data.

It is interesting to note that these values are about the same as those proposed in Section VIII to achieve agreement with the experimental measurements. Although the actual value of 4.5 to 4.56×10^{-4} Btu/ft sec F for k_y is higher than that above, the value of 0.35 Btu/lb F used for C_p is also higher by about the same amount when compared to 0.31. Since these quantities enter as the ratio, k_y/C_p, in the diffusivity, either set of values will yield about the same results.

Measurements of the local heat rate distribution along a molybdenum plate mounted in the same position as the pyrographite

specimen are shown in Fig. C-3 for 10, 20 and 30 seconds after the start of heating. Although the local heat transfer coefficient distribution along the test plate does not vary significantly with time, the temperature difference between the hot gas and the heated surface decreases with time and as a result the heat rate decreases. Since constant heating with time was assumed in the analysis, it was necessary to restrict consideration to results obtained in the early period of heating during which an average constant heat rate distribution was considered to be applicable. For the first 20 seconds after the start of heating reference to Fig. C-3 would suggest a distribution similar to the curve for 10 seconds. However, the temperature of the heated surface of the pyrolytic graphite increases more rapidly than that of the molybdenum. Taking this into consideration led to the selection of the heat rate distribution after 20 seconds of heating as being applicable for the pyrolytic graphite. The third power polynomial shown in Fig. C-3 was fitted to this curve. This was then expanded in the following cosine series for temperature calculations:

$$Q = 55\left(0.546 + 0.312\cos\pi\frac{x}{\ell} + 0.067\cos 2\pi\frac{x}{\ell} + 0.040\cos 3\pi\frac{x}{\ell} + 0.017\cos 4\pi\frac{x}{\ell} + 0.015\cos 5\pi\frac{x}{\ell} + 0.008\cos 6\pi\frac{x}{\ell} + \ldots\right)$$

Comparison of predicted results based on the above values with experimentally measured temperatures is made in Figs. C-4 and C-5. Deviations up to approximately 100 F are to be noted. This amounts to 10 percent at the higher temperatures increasing to 25 percent at the lower.

Such agreement between the theory and experiment may be regarded as satisfactory in view of the strong dependence of the thermal properties of this material on temperature and possible variations from the assumed heating conditions.

It may be noted, for example, in Fig. C-4 that at the heated surface the slopes of the experimental curves at 1/2 and 3-3/8 inches from the leading edge are greater than those of the theoretical curves. This could be due to the local heating rates being higher than the ones used. These differences in slopes are more likely, however, due to the influence of the lower value of k_y at the higher temperatures. The fact that the theoretical curve at the 3-3/8 inch location falls above the experimental through most of the plate also suggests that the local heat rate distribution used in this region or upstream was a little high.

The distributions along the plate shown in Fig. C-5 agree exceptionally well except near the leading edge at the midplane and unheated surface. The fact that the experimental curves at these locations are below the theoretical could in part be due to the effect of the higher values of k_y in the lower temperature range. The average temperatures in the lower half of the plate during the heating period being considered were around 250 to 300 F, for which the curves in Fig. C-1 indicate the value of k_y is above 4.0×10^{-4} Btu/sec ft F. It is also possible that some heat leakage out through the edge of the plate occurred.

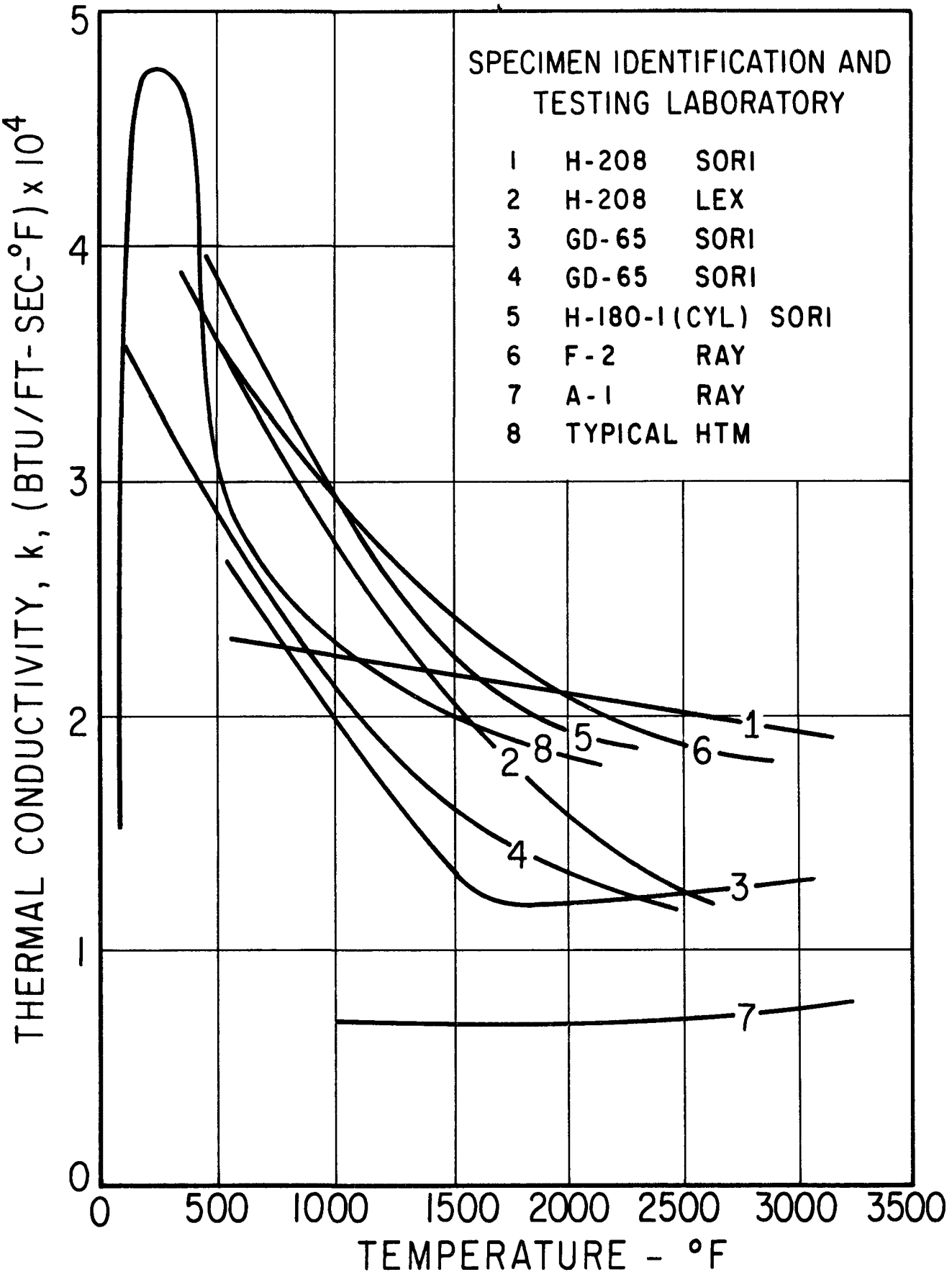

FIG. C-1 SUMMARY OF THERMAL CONDUCTIVITY DATA FOR PYROGRAPHITE IN THE "c" DIRECTION

COURTESY OF LOCKHEED MISSILES AND SPACE CO.

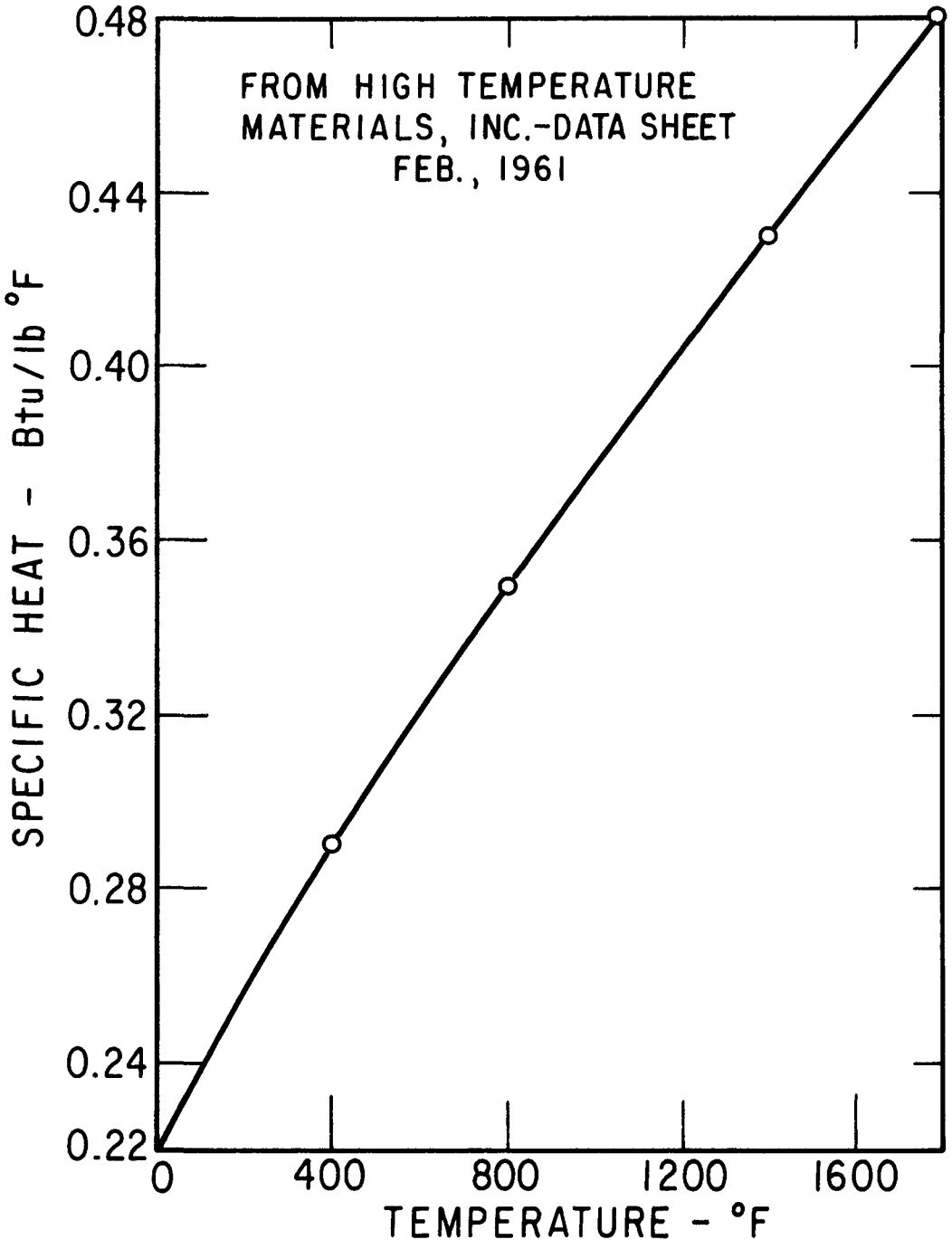

FIG. C-2. SPECIFIC HEAT OF PYROLYTIC GRAPHITE

HYD 7422

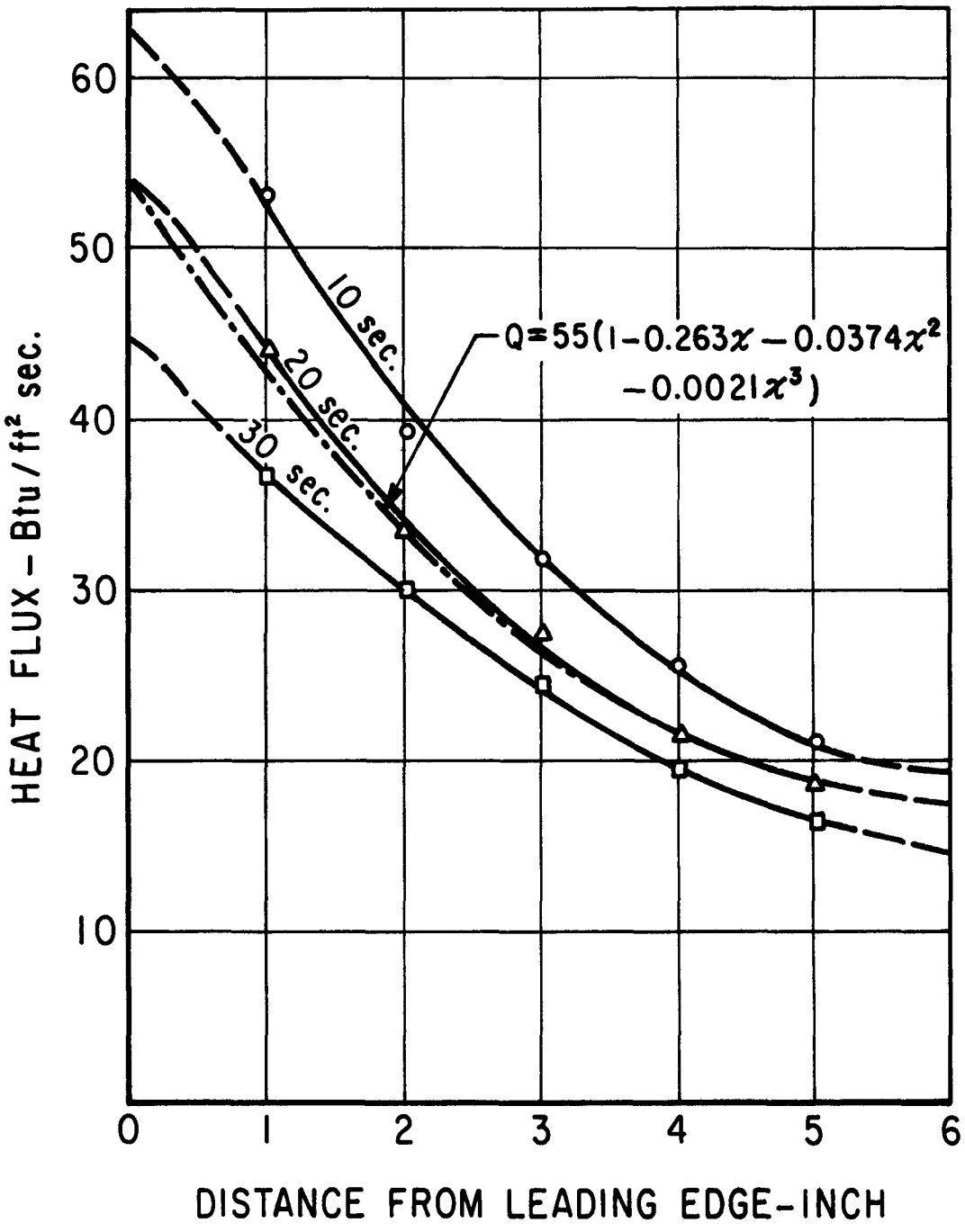

FIG. C-3 HEAT FLUX DISTRIBUTION ALONG HEATED SURFACE DETERMINED FROM MOLYDENUM PLATE MEASUREMENTS

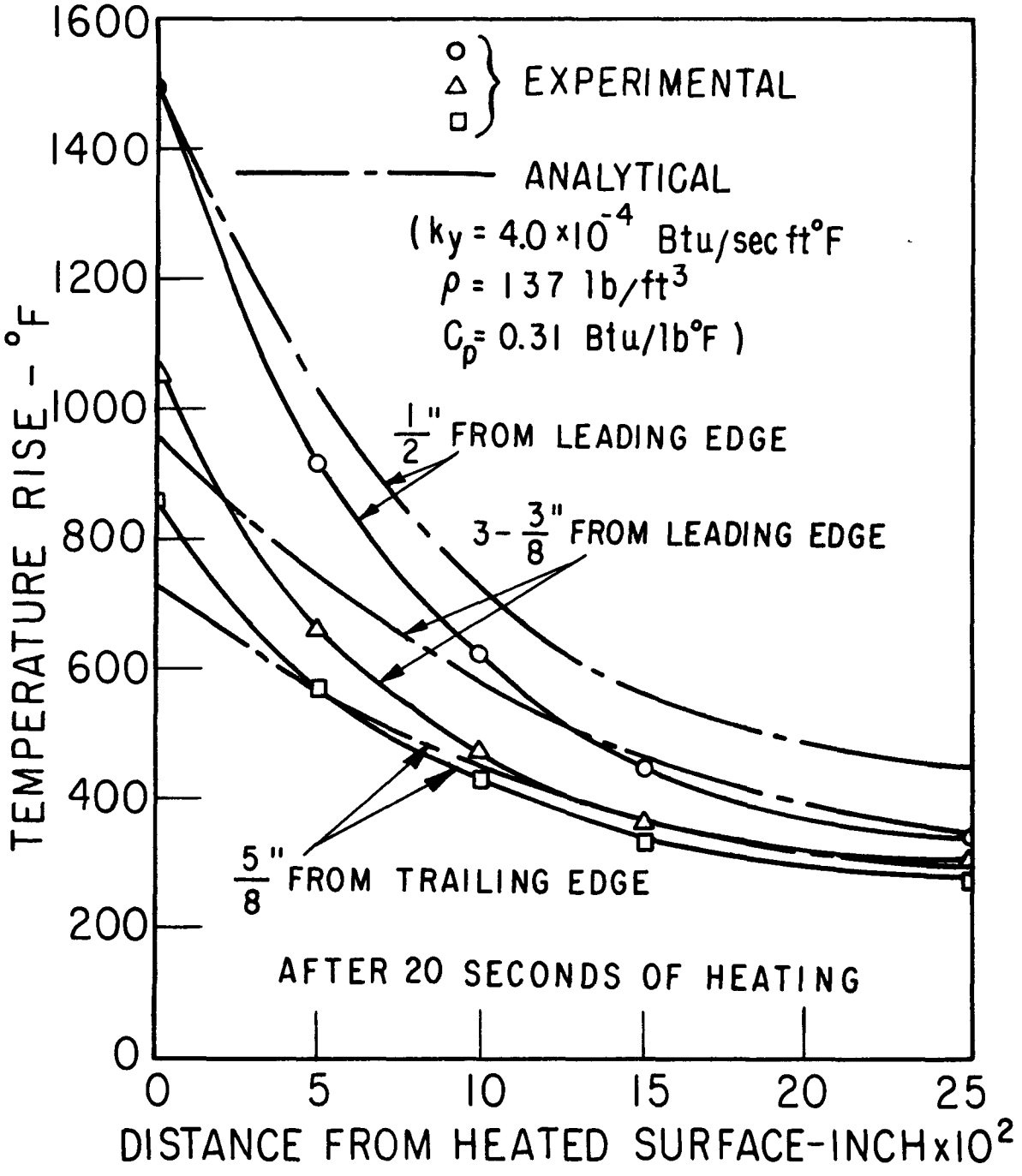

FIG.C-4 PREDICTED AND EXPERIMENTAL TEMPERATURE DISTRIBUTIONS THROUGH A PYROLYTIC GRAPHITE PLATE

HYD 7426

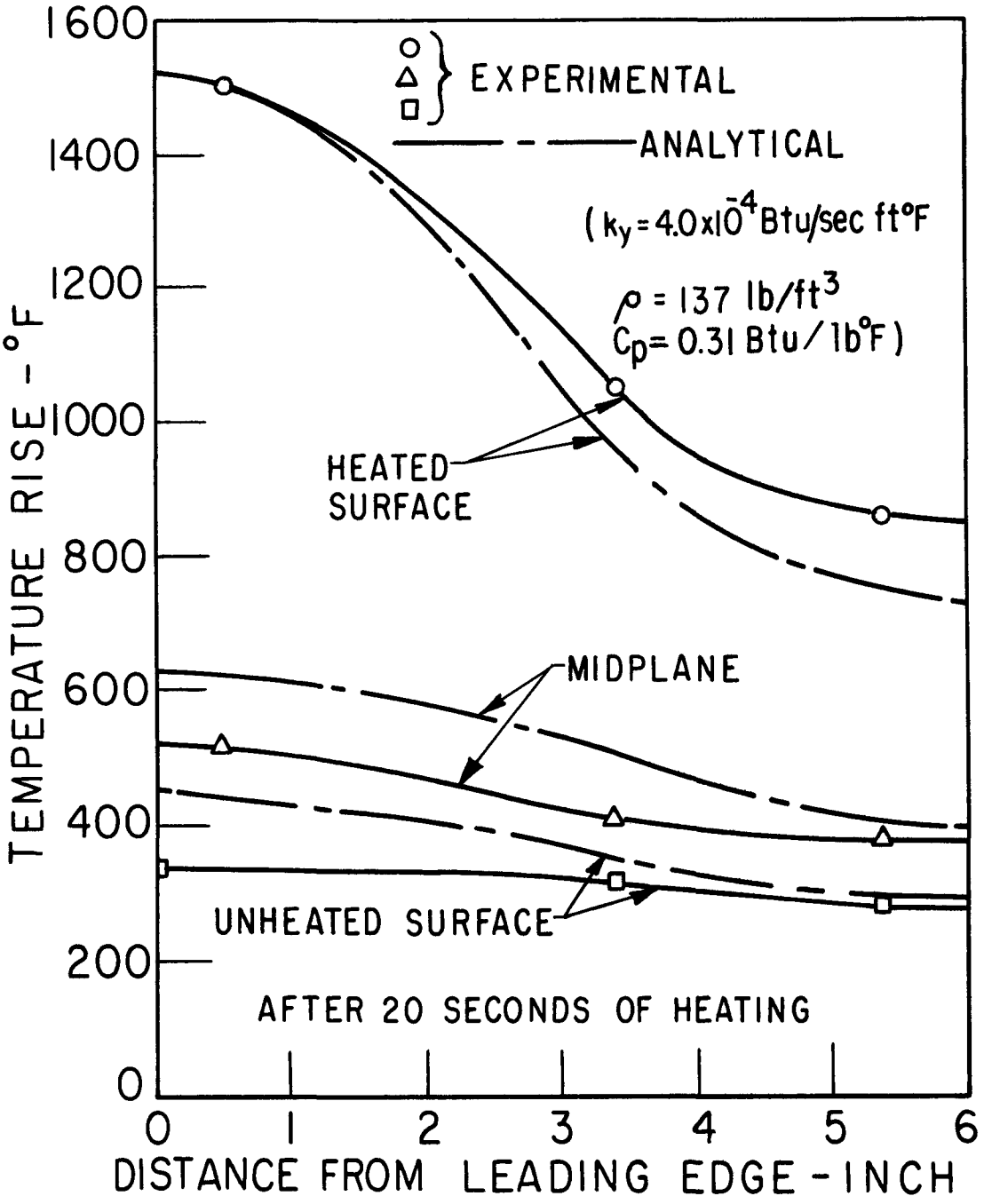

FIG. C-5 PREDICTED AND EXPERIMENTAL TEMPERATURE DISTRIBUTIONS ALONG A PYROLYTIC GRAPHITE PLATE